Master RADMEP

Master *Radiation and its Effects on MicroElectronics and PhotonicsTechnologies* (RADMEP)

Characterization of Radio-Photo-Luminescence (RPL) Dosimeters Under High Dose X-ray Irradiation

Master Thesis Report

Presented by

Afrina Hasan

and defended at

University Jean Monnet

11th September 2023

Host Supervisor: Prof. Matteo Ferrari

Academic Supervisor: Prof. Sylvain Girard

Jury Committee:

Prof. Arto Javanainen, University of Jyväskylä

Prof. Paul Leroux, Katholieke Universiteit Leuven

Prof. Sylvain Girard, University Jean Monnet

Prof. Frédéric Saigné, Université de Montpellier

Erasmus+

Characterization of Radio-Photo-Luminescence (RPL) Dosimeters under High Dose X-ray Irradiation

Master Thesis Report

Afrina Hasan

and defended at

University Jean Monnet

Supervised by-

Prof. Matteo Ferrari

Master Radiation and its Effects on MicroElectronics and Photonics Technologies (RADMEP)

September, 2023

Abstract

Radio-Photo Luminescence (RPL) glasses are used as passive dosimeters, having a wide range of applications in different radiation fields, where low to high doses are absorbed.

This work presents an experimental characterisation of FD-7, a commercial RPL glass dosimeter, irradiated with X-rays at different doses ranging from 0.3 kGy to 0.5 MGy. Investigation over such a broad range allows to enhance the understanding of RPL response in different dose level, out of their normal range of application up to 0.5 kGy. The purpose of this research is to achieve additional information on the response of FD-7 RPL glass dosimeters at high doses, to further their use in extreme high dose environment, especially targeting MGy range. The findings will be beneficial for the European Laboratory for Nuclear Research (CERN), where these dosimeters are used in environments in which such doses can be reached.

In this study, a customized set-up has been developed, allowing the investigation of various relevant quantities, need to be measured in real-time. For instance, Radiation Induced Attenuation and transmittance response during irradiation and their recovery after irradiation are measured. It also allows to perform post-irradiation passive measurements.

Parametric studies have been performed to assess the dependence of these quantities on the total absorbed dose and on the dose rate (ranging between 1.75 Gy/s and 0.175 Gy/s). Their kinetics during irradiation and recovery after irradiation are studied. Additionally, RPL signal evolution during irradiation with total absorbed dose up to 5 KGy at 1.036 Gy/s dose rate has been measured and reported, including settling of RPL signal to a constant intensity after irradiation. The RPL signal is normally used alone to determine the total absorbed dose, this technique being extensively used and considered as reliable up to approximately 0.3 kGy. For higher doses, a combination of both RPL signal and transmitted light is used to determine the total absorbed dose. Therefore, measurement of RPL signal in addition to transmitted signal measurement can provide a more complete view on the investigated phenomena at high doses.

Finally, limitations of RPL dosimetry in certain dose ranges, especially within 0.3 kGy to 6 kGy, usually referred as mid-dose range are discussed based on the collected results and a novel method of combining RIA measurement with transmittance measurement is proposed in this thesis work to improve the accuracy and reliability of RPL dosimetry in this particular dose range.

Acknowledgement

This thesis has been conducted at Laboratoire Hubert Curien (LabHC), France in collaboration with the European Laboratory for Nuclear Research (CERN) in frame of my accomplishment of Erasmus Mundus Joint Master Degree (EMJMD) in Radiation and its Effects on MicroElectronics and Photonics Technologies (RADMEP), specialization in Photonics at University Jean Monnet (UJM), France along with University of Jyväskylä (JYU), Finland; Katholieke Universiteit Leuven (KUL), Belgium and Université de Montpellier, France.

First and foremost, I would like to express my earnest gratitude to my supervisor Prof. Matteo Ferrari for his invaluable guidance, immense support and continuous motivation throughout this master thesis. The completion of this thesis will never be possible without his constructive feedbacks and encouragement.

I would extend my gratitude to my academic supervisor Prof. Sylvain Girard for his valuable feedbacks. I am grateful to Dr. Cosimo Campanella, Assistant Prof. Adriana Morana and Prof. Youcef Ouerdane for supporting me with their expertise in experiments and data analysis. I would offer my gratitude to Dr. Ygor Q. Aguiar, Senior Fellow at CERN for providing useful resources and supporting with RPL readout at CERN. Appreciation goes to my fellow colleague Abrham Kassa Alem for his research regarding Monte Carlo Simulation.

I am thankful to LabHC for providing me good research facilities and to the collaborating institute CERN for providing necessary resources. I would also like to acknowledge all the team members in MOPERE (Materials for Optics and Photonics in Extreme Radiation Environment) group, at LabHC for helping me in every possible way during my internship.

I would also like to appreciate all faculty members and co-ordinators from all the collaborating universities for their guidance and efforts. Finally, I am thankful to European Commission for giving me an opportunity to participate in this amazing masters programme with prestigious Erasmus Mundus Scholarship.

Table of Contents

List of Figures

List of Tables

Chapter 1. Introduction

Dosimetry is a process of monitoring and quantifying absorbed dose or dose rate due to ionizing radiation in radiation field and its interaction with matter [1]. Precise and reliable dosimetry is not only an essential part of medical application, but also it is equally important in any radiation environment to ensure safety for human being as well as for minimizing the radiation effects on materials, electronics and in general every equipment and complex system employed in radiation areas.

In this context, numerous devices have been developed over decays, for the estimation of radiologically relevant quantities. Depending on the specific application, different dedicated dosimetry systems are required, targeting the specific radiation conditions and dose level to be measured. As a result, based on different methodologies, diverse dosimetry systems are available to satisfy the needs of a wide range of radiation environments, such as the ones existing in space, nuclear applications, particle accelerators, medical physics, and concerning the management, and disposal of radioactive waste.

At the European Laboratory for Nuclear Research (CERN), several systems have been developed and are nowadays in use, including beam loss monitor (BLM) system, radiation monitoring (RadMON) system and distributed optical fiber (OF) [2] system to monitor the dose levels in the mixed radiation fields produced by the accelerator complex [3]–[5]. Additionally, different passive dosimeters are placed near radiation sensitive devices to determine the actual dose absorbed in operation [6-7].

Among those passive dosimeters used at CERN, Radio-photoluminescence (RPL) dosimeters are generally considered as promising for having unique features including small size [5], good response with accumulated dose, low energy dependency, reproducibility, non-destructive multiple readout capability and long stability against fading effect [3], [7]–[9]. However, further studies are currently required to enhance the understanding and reliability of RPL dosimetry, especially for their use in high-dose environment and up to doses reaching the MGy level. This need is particularly emerging in recent times, as the radiation levels produced by accelerators and high-power targets progressively increase with the advancement and development of these technologies. Accordingly, the doses delivered to critical materials and components in operation are correspondingly increasing, in many cases reaching the MGy level, making their accurate monitoring vital for the correct operation of the accelerator system [10]. Similar considerations apply to other applications, such as the ones linked to space, nuclear technologies and medical physics.

1.1 Radio-Photoluminescence mechanism

Doping Silver (Ag) in Phosphate glass forms $AgPO_4$ by inducing stable Ag^+ centres uniformly throughout the glass sample [8]. When this type of glass sample is exposed to an ionizing radiation field, several luminescence and absorption centres originate, corresponding to radiation induced point defects. In fact, the interaction between ionizing radiation and glass leads to the creation of free electron-hole pairs by releasing electrons from different ions. for example PO_4^- [8]. The Ag^+ ions present in the glass

can trap these electrons and holes, leading to the creation of two types of luminescence centres: Ag^{0} by capturing an electron and Ag^{++} by capturing a hole as shown in Figure 1. 1 [7], [8]. These luminescence centres are known as Radio-photoluminescence (RPL) centres.

The number of generated Ag^{0} and Ag^{++} centres increase with total absorbed dose in traditional application range up to a few Gy [7], [8], [11]. In addition to RPL centres, absorption centres, also known as color centres are created by ionizing radiation. Like RPL centres, color centres generation rate also increases with increase in absorbed dose [3]. This formation of color centres leads to change in color of RPL samples from transparent to different shades of brown, the higher the dose, the darker the glass [12], as shown in Figure 1. 5 (b). Consequently, the transmittance of glass sample reduces progressively with absorbed dose [3]. The exact nature of color centres in Ag-doped phosphate glass has not been fully investigated yet.

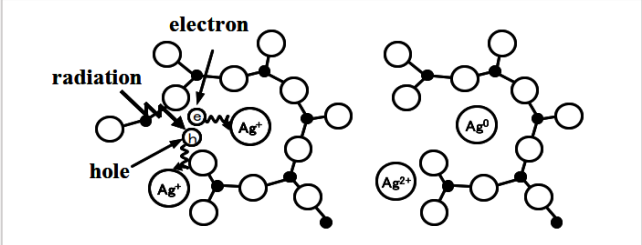

Figure 1. 1: RPL centre formation during irradiation, figure from [7], [8], [11]

$$AgPO_4 \longrightarrow Ag^{+} + PO_4^{-} \qquad [8]$$

By trapping electron, $Ag^{+} + e^{-} \longrightarrow Ag^{0}$ [7], [8]

By trapping hole, $Ag^{+} + h^{+} \longrightarrow Ag^{++}$ [7], [8]

RPL centres can be excited to higher energy state with an Ultraviolet (UV) light source. This excitation is followed by and emission of light in visible range at the time of transition from higher energy state to original centres. Ag^{0} emits blue light at 450 nm and Ag^{++} emits orange light at 630 nm [9]. The whole process is illustrated in Figure 1. 2.

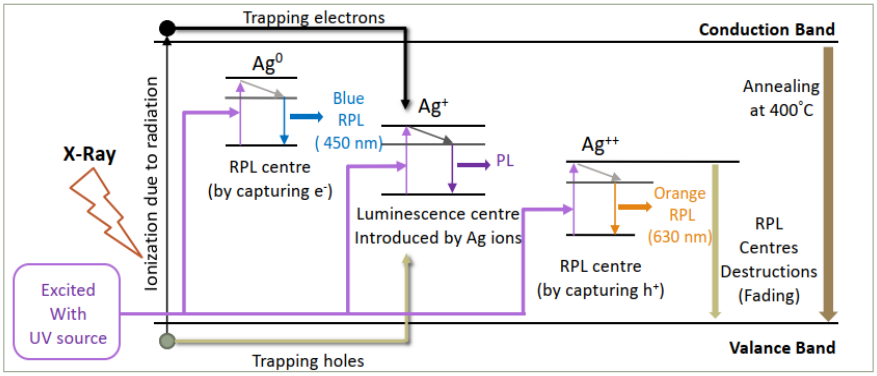

Figure 1. 2: Energy band diagram of Ag-doped Phosphate glass,(Adapted from[7], [8], [11])

The intensity of orange light increases with the absorbed dose up to certain dose level. On the hand, intensity of the blue light is comparatively low and does not change significantly with total accumulated dose or with irradiation time [7]. In therefore, orange RLP signal is considered for the dose estimation.

RPL centres are usually very stable at room temperature [7]–[9]. After irradiation, some of the trapped electrons return to the original valance band naturally, this leading to a degradation of RPL centres with time. This phenomenon is known as fading effect. In standard storage conditions, this fading effect is less than 1% in a month [9]. Exciting the RPL centres with UV light for long exposure times or using powerful lasers might cause fading effect as well.

All the centres can be erased by annealing the sample at high 400° C temperature [7], [8], [11]. The efficiency of this well-established annealing protocols for high dose applications is currently being verified [7], [13], [14]. However, duration of annealing depends on the composition of the material and the total absorbed dose, for instance an irradiated FD-7 glass sample, up to 1 kGy requires 4 hours of annealing for erasing all the centres [15].

1.2 State-of-the arts

RPL signal at 630 nm generally increases linearly with the absorbed dose up to 10 Gy in FD-7 dosimeters. Following the producer's declarations, the dosimetry range can be extended up to maximum 500 Gy [16]. Exceeding the mentioned dose limit causes non-linearity in RPL signal as a function of the total absorbed dose is shown Figure 1. *3*.

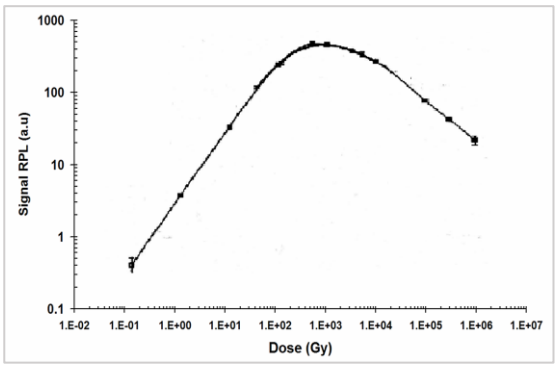

Figure 1. 3: Figure from [17] , evolution of RPL signal with dose

The response of RPL dosimeters can be categorized in three distinct dose regions depending on the RPL signal behaviour.

As extensively reported in the literature, RPL dosimeters are most effectively used in low-dose range, in which RPL signal increases linearly with dose and in which the amount of radiation induced color centres is not relevant [7], [8], [14].

In this work, the possible extension of the usability in dose range of RPL signal is discussed, most of the considerations being based on the findings at CERN. As the absorbed dose increases, other phenomena start to occur, leading to increase in absorption and flattering the RPL curve. Further increase in absorption with total dose

leads to a saturation of RPL signal first, followed by its progressive decrease as a function of the dose, as shown in Figure 1. *3*. This allows the definition of different dose ranges, referred to as low, mid and high dose rates, which are better discussed in the following paragraphs.

The dose intervals defining low, mid, and high dose regions are not precisely specified, this mainly due to the general lack of data at mid and high doses and because they are expected to be depended, at least to a certain extension, on the specific irradiation conditions. Based on the existing literatures, mainly produced by CERN and summarized in Figure 1. 5 (a) , low-dose range extends approximately up to 300 Gy, mid-dose ranges between 300 Gy to 6 kGy and high dose range over 6 kGy [3], [6], [12], [15].

As specified in [3], [6], the RPL signal readout alone allows to determine the absorbed dose in low dose measurement. However, the evolution of color centres with absorbed dose makes the glass sample progressively darker as clearly visible in Figure 1. *5* (b), leading to gradual increase in attenuation of RPL signal due to increase in absorption of RPL light by the color centres. Consequently, in so called mid-dose range, reaching a maximum as a function of the dose and then starts to decay at higher doses. The simultaneous production of RPL centres and color centres, leading to competitive phenomena, makes dosimetry based on the passive measurement of RPL signal alone ambiguous in mid-dose range, as the correspondence between RPL signal and dose is not univocal. Especially around the peak, where the RPL signal is almost flat.

To overcome this problem, transmittance of the RPL glass sample can be measured in addition to RPL signal measurement [4], [12], [13], [18]. This allows the low dose region and high dose region to be clearly distinguished and the ambiguity to be solved in mid-dose range. Higher transmittance, generally close to 100%, is associated to transparent, or almost transparent, glass sample which is associated to the low dose range. By contrast, lower transmittance, generally 1% or even lower than that corresponds to darker or even black samples and is associated to the high-dose range, as shown in Figure 1. 5). Both in low and high dose region, RPL signal exhibits linearity with dose, and accordingly the dose is determined by the RPL signal alone, the transmittance being used only to distinguish the low-dose region form the high-dose region.

Based on these considerations, an adapted readout system combining both RPL and transmittance specifically devoted to high dose measurement has been developed by CERN. Figure 1. 4 shows a schematic diagram of CERN's RPL readout system. From Figure 1. 5 (b), transmittance at 445 nm wavelength progressively decreases with the absorbed dose within mid-dose range that makes this wavelength useful to determine dose is this specific range.

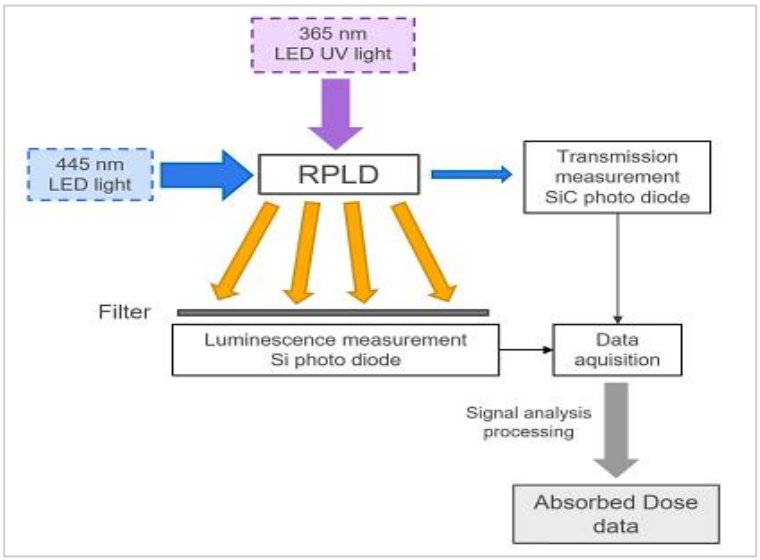

Figure 1. 4: Schematic diagram of RPL readout system used at CERN (Figure from [2])

In this readout system, UV LED at 365 nm wavelength is used to excite the RPL centres and 445 nm LED light is used measure the transmitted light. The readout system used at CERN is applicable for passive characterisation of irradiated RPL sample. This system has been calibrated using ^{60}Co gamma irradiation, taking account the fading effects of RPL centres and color centres, conversion from dose in water to dose in the glass sample in the selected irradiation conditions, as reported in [3]. The calibrated reference curve and some irradiated samples at CERN is presented in Figure 1. 5.

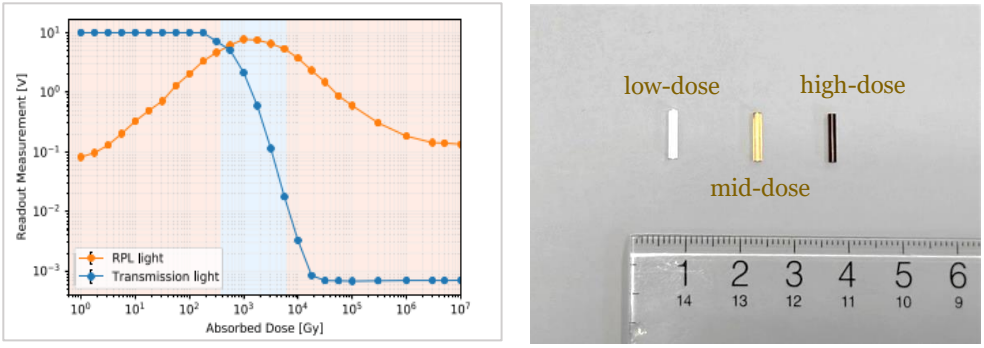

(a) (b)

Figure 1. 5: (a) RPL and transmission light measurement, calibrated in a ^{60}Co gamma field in the Risø HDRL Facility, Denmark (figure from [2]); (b) RPL dosimeters irradiated at CERN

1.3 Motivation and scope of the thesis

RPL glass dosimeters have been proven one of the most promising dosimeters in medical field [8]. As a result, several studies already have been carried out to explore their applications in low dose environments. However, their application in high dose environment still not recognized well.

For passive dosimetry, CERN is using RPL glass dosimeters in several applications in the accelerator system. Usually, the readout of RPL dosimeters at CERN is performed at least after couple of days from the conclusion of the irradiation. As a result, behaviour of RPL dosimeters during and immediately after irradiation is not evaluated the during readout process, which is performed at a later stage. At the same time, the transmittance being so critical for dose assessment in mid-range, it is important to further characterize the response of the dosimeters in real time and in the phases immediately following the irradiation as well.

- design and development of a novel system aiming to evaluate the response of RPL dosimeters both real-time online measurement and offline, which also referred as passive measurement in different literature with the assessment of different quantities.
- validation of the developed system by performing offline (without irradiation) experiments, on both pristine samples and on samples previously irradiated at CERN, to measure the quantities of interest in real-time .
- characterisation of the response of the dosimeters as a function of X-ray irradiation using the sources available at Laboratoire Hubert Curien (LabHC), France
- realization of online measurements to monitor in real-time Radiation Induced Attenuation (RIA), radiation induced transmittance decay along with its recovery after irradiation up to doses in the MGy range
- realization of so-called post-mortem measurements to observe the change in RIA, transmittance decay after a certain time from the conclusion of the irradiation.

Through these investigations, this work aims to enhance the existing knowledge of RPL, especially targeting dosimetry for high dose application.

Chapter 2. Methodology

2.1 RPL Glass Samples

Depending on the composition and concentration of the silver doping, different types of RPL samples are available [8], [19]. Based on the radiation condition present in targeted field, the most appropriate type of sample can be selected [7].

CERN traditionally uses FD-7, a commercial RPL dosimeter, manufactured by a Japanese company named Chiyoda Technology. In view of their current use at CERN, FD-7 glass dosimeters are selected for all the experiments and studies here presented. FD-7 glasses are produced in the form of cylindrical rod-shaped phosphate samples, with a diameter of 1.5 mm and length of 8.5 mm, showing in Figure 1. 5 (b). Material composition of FD-7 glass rod is given in Table 1. Details information can be found in the datasheet [16], provided by the manufacturer.

Table 1: Material composition of FD-7 RPL glass sample [3]

	O (wt%)	P (wt%)	Na (wt%)	Al (wt%)	Ag (wt%)	Density (gm/cm^3)
FD-7	51.16	31.55	11.0	6.12	0.17	2.6041

FD-7 has long stability against fading effects, less than 1% in a month [9], [20]. Moreover, its small size represents an advantage, both in terms of dose resolution and to be conveniently placed nearby elements whose absorbed dose need to be measured [3].

2.2 Characterisation of RPL dosimeters: measured quantities

In this work, several FD-7 samples were characterized during and after irradiation, some assessments extending over several months. The purpose of these investigations is to explore different radiation effects, including Radiation Induced Attenuation (RIA), radiation induced transmittance decay, recovery, post-mortem etc. These quantities are briefly described in the following sections.

2.2.1 Radiation Induced Attenuation (RIA)

During irradiation, RPL glass sample experiences an excessive attenuation of transmitted light, in comparison to the usual attenuation for non-irradiated glass sample, associated to the radiation-induced point defects [21], [22]. This phenomenon is commonly referred to as Radiation Induced Attenuation or RIA. RIA is the most common radiation effect on photonic components and it is extensively investigated for example in optical fibers. RIA can be determined by the formula given below:

$$\mathrm{RIA}\,(t,\lambda) = -\left(\frac{10}{l}\right)\times \log 10\left(\frac{I(t,\lambda)-I_N}{I_{ref}(0,\lambda)-I_N}\right) \qquad (2.\,1)[23]$$

Where, $I_{ref}(0,\lambda)$ is the initial intensity recorded as reference and $I(t,\lambda)$ is the intensity at time t during irradiation at a specific wavelength λ, I_N is the background signal attribute to thermal noise.

RIA described in Equation 2.1 is a function of time and wavelength. Another way to calculating RIA is calculating spectral RIA as a function of dose and wavelength according to the following equation 2.2.

$$\text{Spectral RIA } (D,\lambda) = -(\frac{10}{l}) \times \log 10\ (\frac{I(D,\lambda)-I_N}{I_{ref}(0,\lambda)-I_N}) \qquad (2.2)\ [24]$$

Where, $I(D,\lambda)$ is the intensity signal after a certain dose D, at λ wavelength. This relative measurement RIA for both as function of time and as a function of dose provides value in decibel (dB) per unit of sample length.

RIA is a wavelength and time dependent parameter [21]. Usually, RIA is higher at lower wavelengths [25] and it increases with total absorbed dose. Other factors possibly influencing RIA is dose rate, temperature, type and energy spectrum of radiation, composition of materials, injected light power etc. [21], [26]. One of the advantages of real time RIA measurement or on-line measurement (meaning that they are performed during irradiation) is that it allows to identify the progressive optical absorption peaking due to the precursors and metastable defects happening during irradiation, this not being necessarily possible with post-irradiation measurement alone.

2.2.2 Recovery and Post-mortem measurement

Measurement of RIA at a selected instant of time after irradiation conclusion provides information on the recovery of the radiation-induced metastable defect in the sample material with time. Usually, RIA decreases with time after the end of the irradiation and stabilizes after certain time [15],[18]. This reduction of RIA observed in these conditions is known as recovery. As this can be considered as RIA measurement as well, equation 2.1 is used to determine recovery too. Similar to RIA, recovery also depends on several factors, such as total absorbed dose, dose rate, temperature, time, radiation type.

In the present work, recovery is measured in two different conditions: in the first hours immediately following irradiation, and is referred to as proper recovery, and after a few days or months, in this case being referred to as a post-mortem measurement. For the recovery measurement samples were kept t in the same position under identical conditions as the ones experienced during the irradiation, as described in section 2.5. RIA was generally measured for at least 3 hours starting from the end of the irradiation under these conditions.

On the other hand, the post-mortem measurement was performed in a different configuration and in a different environment, as it was performed after several days or after few months, and accordingly it required the measurement set-up to be re-arranged and realigned out of the irradiation facility, as described in section 2.4. Efforts were made to reproduce the environment and the conditions that resemble the environment during irradiation, to minimize the differences between the set-up used for post-mortem measurements and during irradiation.

2.2.3 Transmittance

Usually, transmittance defined here as T, is the ratio of transmitted light to incident light of any glass or transparent material [27]. T can be calculated by using following general formula:-

$$T = \frac{I_t(\lambda) - I_N}{I_i(\lambda) - I_N} \quad (2.3)[27]$$

Where, $I_i(\lambda)$ is the intensity of incident light and $I_t(\lambda)$ is the intensity of transmitted at λ wavelength. Generally, a transparent glass material transmits most of the incident light and therefore, the ratio of transmitted light and incident light is close to 1, representing 100%. On the contrary, when the glass material is opaque, the transmittance drops to very low values, approaching 0.

When a glass material is exposed to ionizing radiation, various point defects originate, leading to glass darkening [23], [28]. Generally, as the dose increases, more point defects are created and the glass becomes progressively darker [3], [6]. The relevant transmittance of the glass sample in comparison to its initial value correspondingly decreases. This radiation-induced relative transmittance can be determined by using the following equation.

$$\text{Transmittance} = \frac{I(t,\lambda) - I_N}{I_{ref}(0,\lambda) - I_N} \quad (2.4)$$

Here, $I_{ref}(0,\lambda)$ is the initial intensity recorded as reference and $I(t,\lambda)$ is the intensity at time t during the irradiation at a specific wavelength of λ and I_N is the background thermal noise signal. The set-up used in the present work to measure real-time RIA evolution with dose allows the relative evolution of the transmittance with time to be measured using Equation 2.4. This equation allows to measure the change in transmittance due to radiation (during irradiation and following recovery). In this work, this parameter is simply referred to as 'transmittance'.

Usually at CERN, transmittance at 445 nm wavelength is measured to distinguish the high dose range from low dose range as well as to quantify the dose in the mid dose range [3], [6].

2.4 Set-up used for Offline RIA measurement

2.4.1 Set-up description

A customized set-up has been developed in the frame of this work to perform offline and post mortem measurements of irradiated FD-7 samples. A scheme of the complete set-up is shown in Figure 2. 1.

In this developed system, a DH-2000 Deuterium-Halogen light source from Ocean Optics, referred to as White Light Source (WLS) is used as a multi-wavelength source ranging from Ultra-violet (UV) to near infrared (NIR) (around 200-1000 nm). Light was transmitted through the RPL glass sample at all the available wavelengths. QE-Pro 38011, a spectrometer with a high resolution, has been used to detect the transmitted

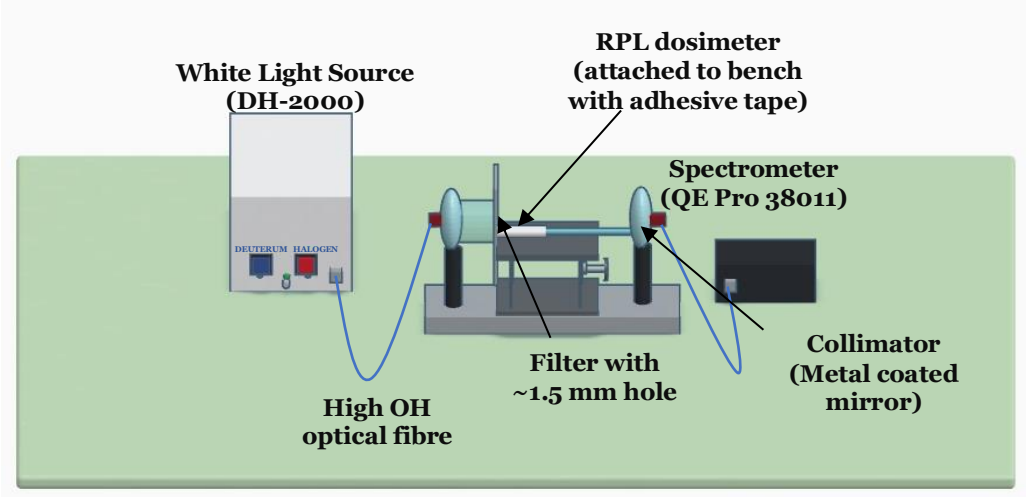

Figure 2. 1: Set-up developed for offline RIA measurement of RPL samples

light. To transfer light through the dosimeter, at first light is guided through high OH fiber from the WLS to the metal coated mirror, working as a light collimator. Further, the collimated light beam is transferred in air without any guide and passes through the dosimeter, that is longitudinally placed on the bench. The position of the mirror is manually adjusted using nobs to let the light pass through the samples. The light transmitted through the sample is then collected by another aligned collimator and transferred to the spectrometer using another high OH fiber again, of the same type of the previous one.

2.4.2 Main Challenges in the set-up and solutions

The alignment is a delicate aspect of this set-up because repeatability is not obvious, as the light has to pass through the sample 'in free space' without the support of the fibers. The concept of using adjustable collimators which makes the alignment convenient is adapted from the methodology described in reference [23], which demonstrates the characterization of a bulk glass sample under X-ray irradiator.

An additional challenge arises with this set-up, especially related with the beam size. In this configuration, the beam size of the transmitted light depends on the diameter of the mirror. As the diameter of the mirror is larger than the diameter of the sample, transmitted beam size is larger than the sample diameter. Consequently, the signal received by the spectrometer includes not only the light that passed through the sample, but also the light that directly reaches the spectrometer unperturbed. As the aim is to collect only the light transmitted through the sample, the light directly reaching to the spectrometer represents an unwanted contribution, leading to inaccuracies in measurement. To overcome this problem, a filter with a hole having a diameter lower than 1.5 mm (that correspond to the diameter of the sample) is placed before the sample to ensure that the light only pass through the hole and guides through the sample. Different types of filters made of different materials have been employed and tested to verify the usability of the developed set-up. All the tested filters are shown in Figure 2. 2.

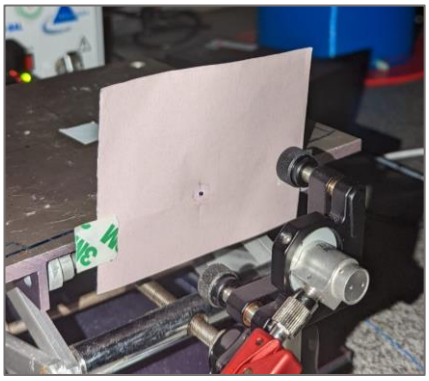

(a) thin paper sheet

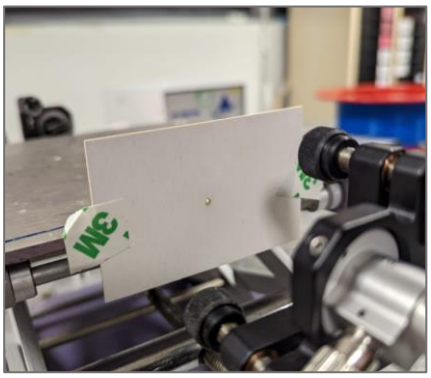

(b) thick paper

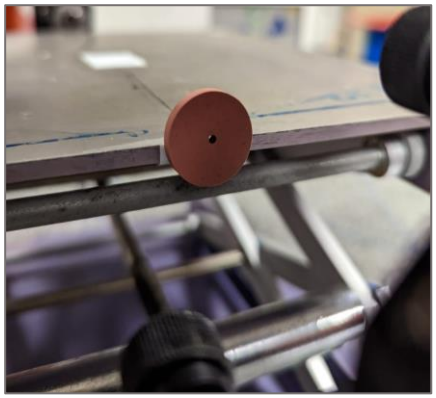

(c) circular structure

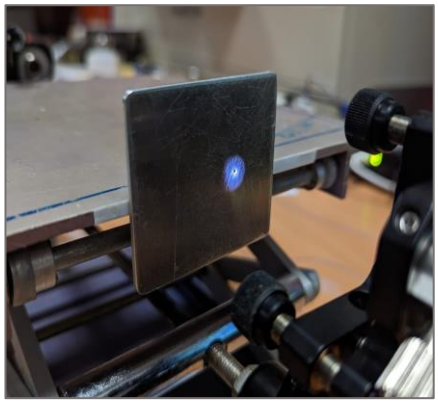

(d) metallic sheet

Figure 2. 2: Different types of filters to block the excess light

Initially, paper sheets were tentatively used as filter as shown in Figure 2. 2 (a) and (b). Notwithstanding, thin paper was not sufficiently stable to effectively conduct the experiment. Besides, making a hole of less than 1.5 mm in a paper sheet is not obvious, and the hole tends to become larger and opaque (for thick paper) with use, especially at the time of replacing the tested sample with a new one. Accordingly, repeatability is not granted in this configuration.

In next step, a circular structure available in the laboratory and containing a hole in the centre (see Figure 2. 2(c)) was used. Although, this set-up shows an improved stability in comparison to the previous ones, the hole diameter was larger than 1.5 mm. As a result, it also turned out unsuitable for the experiment. Afterwards, a metallic plate available in the laboratory with a hole having diameter less than 1.5 mm, shown in Figure 2. 2 (d) has been employed. This metallic plate effectively filtered out the excessive light while allowing a part of light to propagate through the sample.

FD-7 glass samples, both pristine to be used as a reference and another, that previously irradiated at CERN were used to test the stability and repeatability of the RIA measurements performed with this set-up. Although, the repeatability of the RIA measurements obtained with the set-up with metallic plate filter was very high with only 1-2% deviation, the sample alignment was quite difficult and time consuming.

2.4.3 Main Challenges in the set-up and solutions

To overcome the problem mentioned in Section 2.4.2 and based on the knowledge acquired from preliminary set-up, a new sample holder embedded with filter was designed to address the issue previously discussed. This customized metallic piece is designed, aiming to satisfy the following required features in the frame of this work:

- Easy, repeatable, and effective sample alignment;
- Excess light filtering;
- Radiation resistance
- Possible temperature control (if needed);

The proposed design is shown in Figure 2. 3 (a) and the fabricated structure according to the design is shown in Figure 2. 3 (b).

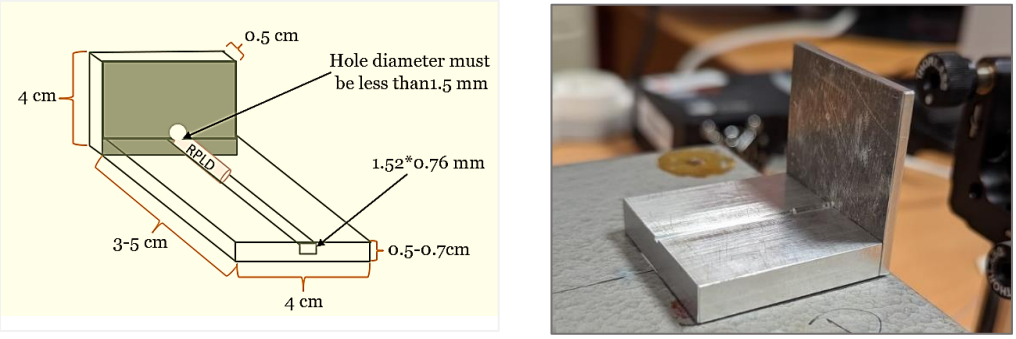

(a) (b)

Figure 2. 3: (a) Design of sample holder embedded with a filter having a hole of ~1.5 mm diameter, (b) fabricated sample holder

The set-up shown in Figures 2.3 (b), a holder structure with a dedicated sample housing and incorporating a filter with a hole of 1.0 mm has fulfilled all the requirements listed in previous paragraph. The holder is entirely realized in aluminium, making it radiation tolerant and allow for possible temperature controls, for example with the use of a heating plate.

The usability of this sample holder has been verified with offline measurement with samples irradiated at CERN. The reproducibility of the set-up using this customized sample holder is comparable as the one of the previously discussed set-up with metallic plate filter, having 1-2% deviation. However, it solved the problem regarding identical alignment in different experiment and improved reliability significantly.

Although, this RIA measurement set-up has satisfying reproducibility, stabilizing the set-up is still challenging. Establishment of a compact set-up in future can improve the stability.

2.5 Online RIA measurement

2.5.1 Dose homogeneity in RPL sample

Typically, the dose deposition in a bulk glass sample having dimension exceeding the mm range under X-ray irradiation is not homogeneous over the sample volume, and accordingly the produced defects are also inhomogeneous. This phenomenon has already been observed in previous experiments [23]. This inhomogeneity depends on the specific X-ray fluence energy spectrum used for the irradiation, on the thickness of the sample and on the material density and composition. A systematic approach to this complex topic falls beyond the scope of the present work, and was approached in another study, in which Monte Carlo simulations have been used to study the dose deposition in different configurations. The dose deposition in FD-7 sample, having 1.5 mm depth is highly inhomogeneous, compromising the dose readout

X-ray tubes produce photons with a range of energies, varying from low-energy to the maximum corresponding to the energy of the electrons impinging on the target, in this case 100 keV [29]. Low-energy photons in this spectrum are strongly attenuated by the RPL sample thickness and deposit most of their energy on the sample top layers, in the first 0.1-0.5 mm of sample, results in gradient in the distribution of radiation-induced defects corresponding to inhomogeneous dose distribution within the sample.

Homogeneity in dose distribution can be greatly improved by introducing shielding to reshape the X-ray energy spectrum by employing a 1.5 mm thick Al filter, according to [30].

2.5.2 Set-up for online measurement

For real-time Radiation Induced Attenuation monitoring, full set-up was installed inside the X-ray radiation chamber, except light source and spectrometer, following the same procedure described in Section 2.4.1. Details are shown schematically in Figure 2.4.

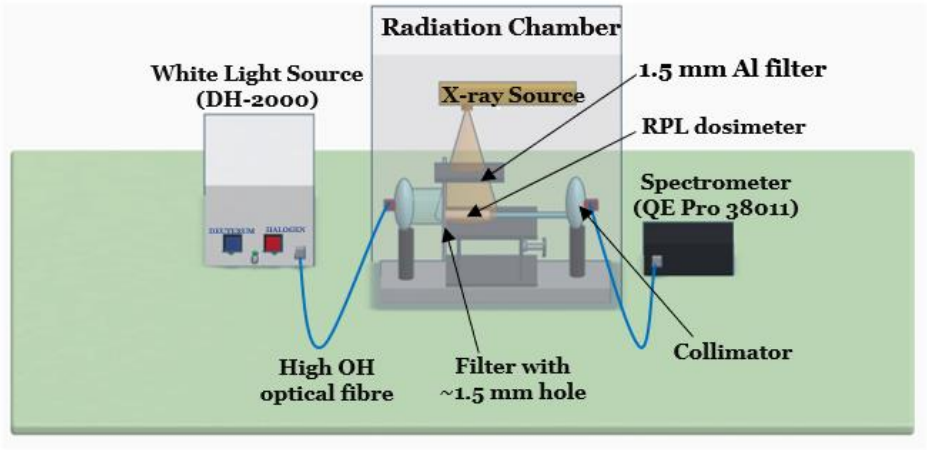

Figure 2.4: Set-up for online RIA measurement of RPL samples under x-ray irradiation

In the present work, the FD-7 samples were irradiated using MOPERIX and IDFix facilities available at Laboratoire Hubert Curien of the University Jean Monnet in Saint-

Etienne, France. Both the sources have tungsten target X-ray tubes operating at a tension of 100 kV and maximum available current of 45 mA.

After implementing the setup inside the irradiation chamber, white light source and spectrometer were connected to the collimators from the outside of the irradiation chamber through high OH fiber. Complete setup inside both IDFix and MOPERIX irradiation chambers are shown in Figure 2. 5.

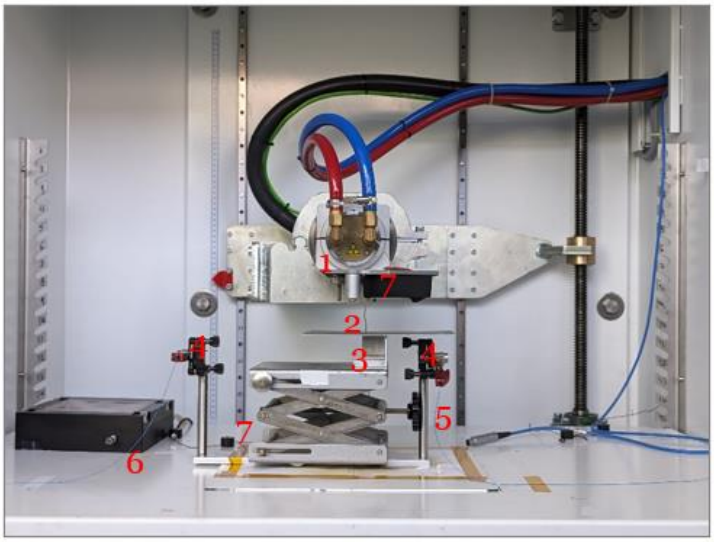

(a)

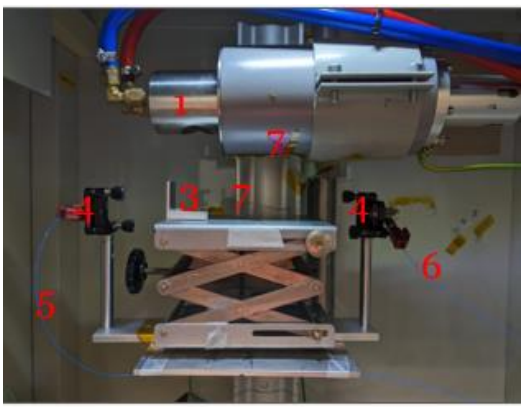

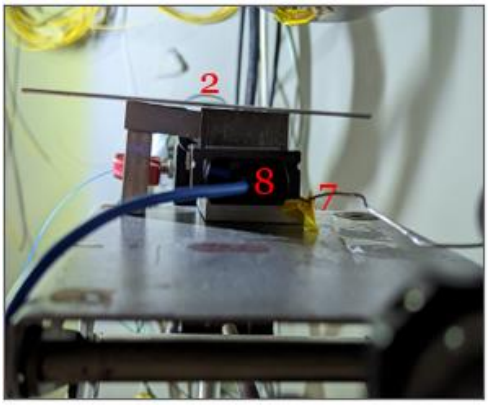

(b) (c)

Figure 2. 5: Set-up for online RIA measurement under x-ray source at (a) IDFix facility and at MOPERIX facility (in (b) without Al filter, in (c) with Al filter) at LabHC; in all pictures: (1) X-ray source, (2) 1.5 mm Al filter on support, (3) sample holed with filter containing sample; (4) collimators, (5) and (6)high OH fiber to inject and collect transmitted light accordingly, (7) thermocouples at different place, (8) ionizing chamber on sample hold

2.5.3 Dosimetry and sample positioning

After set-up installation , the sample position was marked and the dose rate was correspondingly measured with a commercial ionizing chamber, PWT-23344, having a

sensitive volume of 0.2 cm^3 and 2 cm diameter. Details of this ionizing chamber is available in [31]. Typically, an ionizing chamber is a gas-filled chamber containing two electrodes. When the ionizing chamber is exposed to radiation field, having enough energy to ionize the gas molecules, free electron-holes are created and collected by the electrodes. Based on the number of collected charge, ionization chamber provides an output value of absorbed dose rate in water.

The sensitive area of the dosimeter is much larger than the sample's size. Therefore, multiple dose rate measurements were performed by moving the ionizing chamber 1 cm in every direction, to have a rough estimation of the dose gradients at the sample position and of the maximum deviation. The error in dose rate due to the resolution of the chamber in comparison to the sample size and to the sample position was less than 5% for all the experiments. After completing dose rate measurement, the sample holder was mounted on the marked position and the sample was placed longitudinally on it. Due to less dose rate deviation across the sample volume, the dose deposition on the sample in longitudinal direction is considered uniform. The different thickness of the ionizing chamber and of sample holder was compensated to adjust the distance between X-ray source and calibrated position, ensuring that the distance between the source and the sample correspond to the distance between the source and the sensitive part of the ionisation chamber.

2.5.4 Stability of the set-up

This set-up is highly sensitive to any kind of movement of any of its components. Therefore, stability of the source was verified and all the connections were checked prior to each measurement to ensure accurate and reliable data acquisition. Additionally, tree thermocouples were placed during each irradiation: the first one is positioned next to the sample, the second one is attached to the source and the third one is placed in a reference position inside the irradiation chamber. These thermocouples were employed to monitor the temperature variation on sample, source, and environment throughout the experiment time.

Data recorded with thermocouples for all the performed experiments show that temperature variation on the sample fluctuates between 23°C to 28°C depending on the irradiation duration and surrounding temperature. No significant temperature effect on the measured quantitates was reported due to this temperature variation, which is in any case much smaller than the temperature at which annealing effects are observed.

However, environmental temperature can have an impact on recovery in a long run as well. In this present study, irradiated samples were not preserved in a well-controlled environment If future studies will aim at precisely assessing the response of the dosimeters during and after irradiation as a function of the temperature, it will be necessary to perform irradiation at temperature-controlled conditions and to carefully store the irradiated sample in a thermal and humidity-controlled atmosphere, to maximise the stability of created defects over long time.

2.6 Set-up for RPL measurement

Radio-photo luminescence signal acquisition requires a dedicated set-up containing a UV laser source to excite the RPL centres and a highly sensitive photodetector capable of detecting low-energy signals, such as photomultiplier.

In the setup established at LabHC, a high-power laser from Thorlabs (LP405-SF10), having a central wavelength of 408 nm (near UV range) was used. The output power of this laser can be varied up to 11 mW by adjusting the operating current from a threshold current of 22.7 mA to maximum current of 54.5 mA. As the wavelength of this visible laser is very close to UV range, its power was sufficient to effectively excite the RPL centres. A scheme of the developed set-up is reported in Figure 2.6.

The laser used in the set-up is a single mode fiber coupled laser. Therefore, at first, the single mode pigtail is connected to the high OH fiber with a connector. Afterward, similar to the RIA measurement described in section 2.4, the laser light is transported though a high OH fiber to the collimator and injected into the glass sample. However, if the outcoming signal is directly injected in the second mirror, in the same configuration used for RIA measurement set-up, as described in section 2.4 the signal saturates in the spectrometer, as the laser pulse intensity is too high and directly entering to the mirror. This problem can be solved by either placing a filter that can remove the laser pulse from the transmitted spectra or collecting RPL light from a different direction avoiding the direct laser light and minimizing its contribution in the signal detected with spectrometer. As no suitable filter was available to remove the laser pulse, the high OH fiber was placed on the side of the sample, and the second mirror was not used.

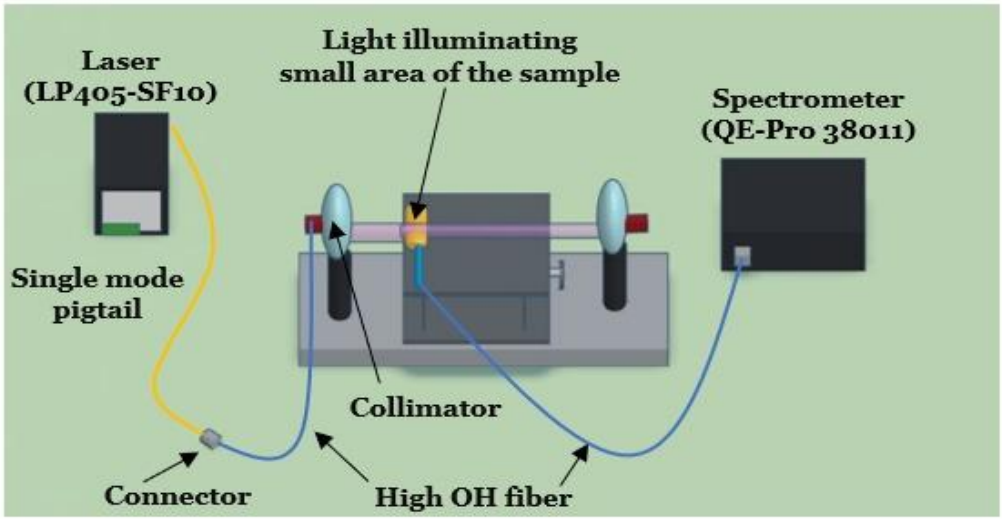

Figure 2. 6: Set-up developed for RPL measurement, also can be used for offline readout of irradiated sample

As photomultiplier is highly sensitive and no filter has been used to remove signal at 408 nm, the laser signal could saturate the photomultiplier. To avoid this issue, QE-Pro 38011 spectrometer was used to collect the RPL signal instead of photomultiplier.

Integration time of the data acquisition was set in such a way so that the laser light could not saturate the spectrometer.

However, due to small collimated beam, the laser light illuminates only a reduced volume of the sample, and accordingly it could only excite a small fraction of the existing RPL centres (in Figure 2. 6). This results in a relatively low and difficult to detect RPL signal. To address this limitation and aiming at maximising the intensity, the sample was illuminated diagonally, as shown in Figure 2. 6 .

The intensity of the RPL signal also depends on the injected light power. The higher the laser output power, the higher the RPL intensity. However, illumination on the sample with high power laser can induce bleaching to the RPL centres too in order to avoid photobleaching, the optimal laser power and excitation time needed to be verified through passive measurement on previously irradiated samples before using it for experiment.

The described set-up is suitable for off-line RPL readout on previously irradiated samples, and can be used to evaluate photobleaching and temperature effects. For online RPL measurement, whole set-up except the laser and the spectrometer was installed under the x-ray source; laser and spectrometer were connected from outside of irradiation chamber through high OH fiber (as for the online RIA measurement set-up, as described in section 2.5). As the fiber used to collect the RPL signal was simply placed next to the sample, it was covered with a lead plate according to Figure 2. 7, in order to minimise radiation-induced effects on the fiber itself, which is not radiation hard.

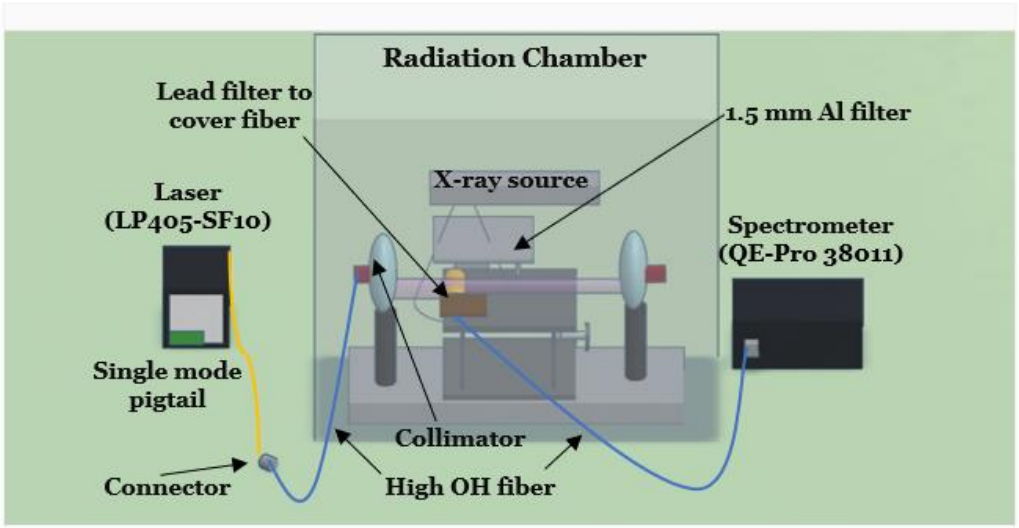

Figure 2. 7: Set-up for online RPL online measurement

The actual set-up is shown in Figure 2. 8. In the figure, sample is not visible as it is blocked by the lead plate. Moreover, 1.5 mm Al filter was placed on the support later which is also not shown in Figure 2. 8.

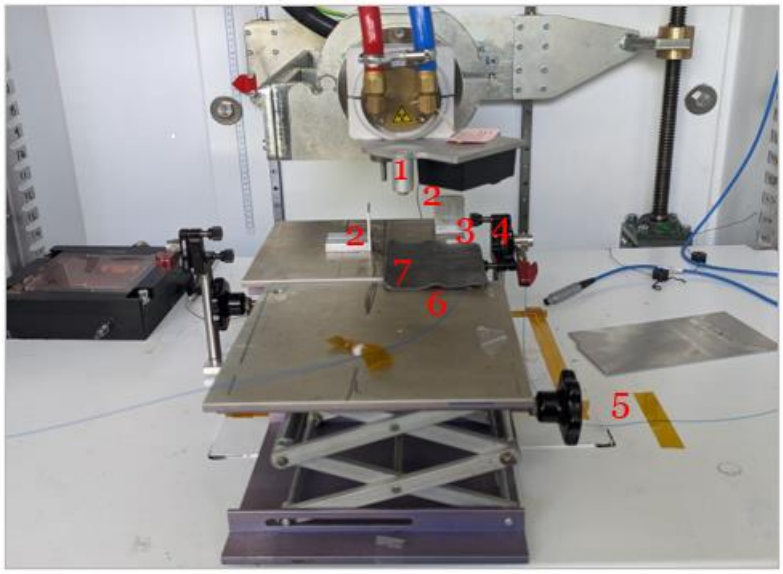

Figure 2. 8: Set-up for online RPL signal measurement under x-ray source at IDFix facility at LabHC; (1) X-ray source, (2) supports to place Al filter (placed later), (3) sample (behind lead filter); (4) collimator, (5) and (6) high OH fiber to inject and collect transmitted light accordingly, (7) lead filter covering the fiber (thermocouples are not visible)

2.7 Confocal microscopy

The distribution of radiation induced defects throughout the sample and its possible inhomogeneities cannot be evaluated by visual inspection. However, samples can be scanned with a confocal microscope allowing to visualize the light emitted by RPL centers and accordingly to estimate the density of the induced defects within the sample volume.

In this regard, passive RPL measurement was performed for irradiated FD-7 samples (both with Al filter and without Al filer) using LabRAM Aramis, a confocal microscope available at LabHC, France. This system consists of a HeCd laser, source operating under CW excitation at 325 nm; a 40×NUV microscope objective and a high-resolution CCD camera.

The laser light was injected to the sample longitudinally with a confocal hole of 150 μm. The emitted spectrum was at first, separated into constituent wavelength by selecting grating 150 and the detected with CCD camera. Cartography was performed to collect spectral emission from different lateral point that corresponds to the density of the radiation induced defects, step size was 100 μm and emitted spectrum was recorded for a spectral range from 400 nm to 900 nm.

Chapter 3. Results and Discussion

3.1 Irradiation plan

In this frame of work, a variety of irradiation experiments were performed using X-ray irradiation, aiming at characterizing the response of RPL dosimeters in a wide range of doses and dose rates and in different irradiation conditions.

In the first irradiation, a single FD-7 dosimeter was irradiated at a total dose of 14.44 kGy(H_2O) without placing any Al filter, in order to investigate RIA in addition to transmittance evolution at different wavelengths and different doses both during and after the irradiation. As RIA measurement for such type of sample has never been performed before, this preliminary study provides valuable insights about the behaviour of these dosimeters in the conditions, as reported in Section 3.2. This irradiation was also helpful for the planning of the following experiments, in which the Al filter was introduced, and in which the dose and dose rate dependency was assessed in different conditions. The purpose of using a 1.5 mm Al filter in all experiments except the first one is to achieve better uniformity in dose distribution throughout RPL samples. Total dose and dose rate for those experiments were converted in equilibrium to FD-7 material according to the process described in Section 3.3, results were expressed in a unit of Gy for dose and Gy/s for dose rate.

In a second irradiation campaign, 4 dosimeters were irradiated with Al filter configuration (in Figure 2.4), aiming at assessing dependency of the selected quantities as a function of the dose, ranging between 1.3 kGy and 0.47 MGy. The irradiation plan is summarized in Table *2* and discussed in Section 3.3.

In a third irradiation campaign, another 4 dosimeters were irradiated in the same shielded configuration to assess the response dependency on the dose rate, ranging between 1.75 Gy/s-0.0175 Gy/s. The irradiation plan is summarized in Table *3* and the results are discussed in Section 3.4.

In a fourth irradiation experiment, detailed in Section 3.6, mid-dose range were targeted. 4 samples were irradiated using IDFix facility at different doses, ranging from 0.37 kGy to 5.10 kGy at a dose rate of 1.036 Gy/s to investigate the different dose effect on transmittance and recovery in this range. Two more samples were irradiated at 0.2072 Gy/s dose rate (5 times lower than 1.036 Gy/s) to observe the dose rate effect in these conditions.

Moreover, a fifth irradiation experiment is dedicated to online RPL readout has performed for 2 samples irradiated at 1.06 kGy and 5.28 kGy total absorbed dose to observe the evolution of RPL signal during irradiation and stabilizing to a fixed value afterward. Results are discussed in section 3.8.

Additionally, dose distribution within two samples, one irradiated with 1.5 Al mm and another without any filter has been observed using confocal microscope, as reported in Section 3.9.

To verify possible radiation effects on the setup, it was irradiated without any sample up to 54 kGy. Results shows satisfying stability throughout the irradiation time, confirming the possibility of using these transport fibers for RPL irradiation at high doses, suggested that the fibers have to be kept sufficiently far away from the source or they should be adequately shielded.

3.2 First irradiation without Al filter: RIA and recovery

During the first irradiation, one FD-7 sample was irradiated under X-ray source available at IDFix facility at a dose rate of 3.99(∓0.31) Gy(H_2O)/s for 1 hour 16 seconds. Recovery was measured for 30 minutes after irradiation. Consequently, total accumulated dose at the end of the irradiation corresponds to 14.44(∓0.11) kGy(H_2O).

In Figure 3. 1 (a), the transmitted signal, expressed in total photon count as recorded with the spectrometer, has been plotted at each wavelength from 240 nm-1000 nm for a selection of representative dose values ranging from 0 kGy(H_2O)) to the maximum dose (14.44 kGy(H_2O). As the total absorbed dose increases, transmitted signal progressively attenuates due to radiation-matter interaction. The shape of the transmitted signal depends on the guiding medium, for here it is high OH fiber and on the source. However, it does not affect the RIA.

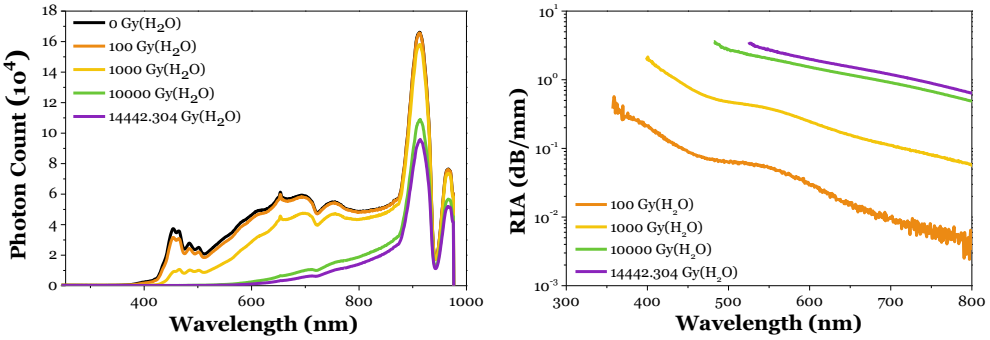

(a) (b)

Figure 3. 1: (a) Transmitted signal as a function of wavelength during irradiation, and (b) spectral RIA at different dose level.

Spectral RIA as a function of the dose for representative dose values is shown in Figure 3. 1 (b). The wavelength range is selected between 300 nm-800 nm, as signals out of this wavelength range have intensities comparable to noise level, resulting in unreliable RIA values. As expected, RIA progressively increases with total absorbed dose. Also, RIA exhibits higher values at lower wavelength, as expected from the literature [25]. Two absorption bands peak are visible: one around 550 nm and another around 380 nm. However, the origin of these absorption peak cannot be identified with RIA measurement alone.

The absorption peak around 550 nm wavelength exhibits gradual reduction with increase in total dose and eventually disappears at higher doses. As a possible explanation for this evidence, this absorption peak might result from the absorption of

transmitted signal by created metastable defects or from precursors site, presents in the pristine sample already and converts to other form during irradiation [21], [32].

As the total absorbed dose increases, the precursors may undergo transformation into other forms through radiation interaction or, may be metastable defects become stable with progress of time, leading to disappearance of absorption peak at high dose. Further studies are required to identify the exact origin of these absorption peaks.

It is recalled that in this irradiation, the Al shielding was not used, resulting in a highly inhomogeneous dose distribution across the sample volume. For this reason, the conversion of the dose in water to dose in the dosimeter is not performed for this sample, as the average dose absorbed by the sample does not consider the inhomogeneities and could lead to misleading interpretations if compared with samples irradiated in shielded conditions.

RIA kinetics has been plotted in Figure 3. 2 (a), including both RIA during irradiation and the following recovery for 30 minutes. For this reason, RIA is plotted as a function of the time. During irradiation, as the dose rate was kept constant, the absorbed dose is proportional to the irradiation time. The plot is limited to 6 wavelengths, selected among others according to the following criteria:

- 445 nm: the wavelength used at CERN to identify different dose range [3];
- 500 nm, 560 nm, and 600 nm: they are near to the absorption peak;
- 700 nm and 800 nm: higher frequencies selected at a regular interval.

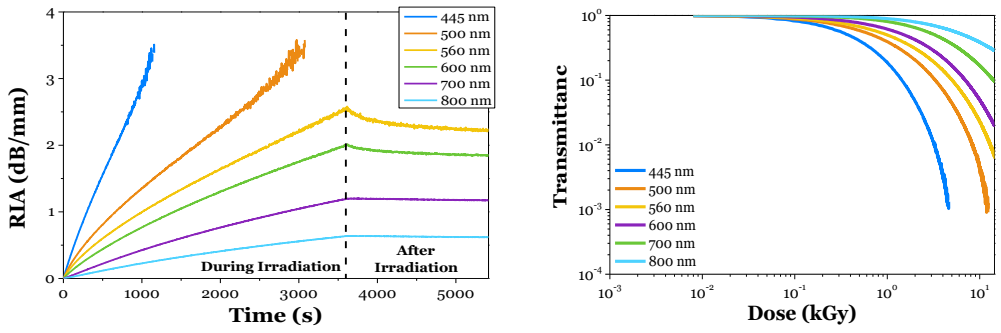

(a) (b)

Figure 3. 2: (a) RIA Kinetics during and after the irradiation, (b) transmittance as a function of absorbed dose during irradiation

RIA at all the selected wavelengths increases progressively with absorbed dose. Eventually, the RIA growth stops at the end of the irradiation and starts to reduce after irradiation above 560 nm wavelengths. On the other hand, transmittance decays with total absorbed dose. The RIA growth and transmittance decay during irradiation and its recovery afterwar is not same for all the wavelengths. Findings from Figure 3. *2* is listed below:

- As the total absorbed dose increases, more color centres are created. Consequently, at all the analysed wavelengths RIA increases correspondingly as a function of the total absorbed dose.
- Both RIA growth and transmittance decay are comparatively higher at lower wavelengths. As a result, transmitted signals at 445 nm and 560 nm become entirely absorbed by the color centres due to higher RIA before reaching to total dose of 12 kGy(H_2O).
- Depending on the wavelength, recovery is possible.

However, RIA value cannot be quantified anymore at values exceedingly approximately 3.5 dB/mm for 445 nm and 650 nm, as the values becomes comparable to noise, leading to high fluctuations and the calculated result gives unreliable values.

These general findings from first experiment provide valuable insights into overall behaviour of FD-7 sample during radiation exposure and subsequent after effects on its properties. It should be recalled that these results were collected in irradiation conditions in which a large dose inhomogeneity is expected across the sample volume. For this reason, it is not possible to directly compare them with the results of the other irradiation campaign quantitatively in respect to the dose. Qualitatively, the results correspond to the ones collected in the other irradiations, that are discussed in the following sections.

3.3 Second irradiation experiment: dose dependency at constant dose rate

Four FD-7 samples were irradiated at MOPERIX facility at a constant dose rate of 0.58Gy (H_2O)/s, as measured with the ionisation chamber, for different durations, aiming to observe the different dose effect on RIA growth and transmittance evolution during irradiation. A 3-hour long recovery was recorded for each sample to quantify the kinetics. During this irradiation campaign, a maximum of almost 0.5 MGy of absorbed dose were achieved for one sample, irradiated for a total of 60 hours, continuously.

Monte Carlo simulations performed in the frame of another study and validated by experimental readout performed at CERN suggest that average total absorbed dose by FD-7 dosimeter irradiated with a 1.5 mm thick Al filter in these irradiation conditions is 3.7 times higher than and the dose in water at the equilibrium [30]. This factor has been used in the present work for all the irradiation under Al shielding, to convert the dose rate in water provided by the ionization chamber, used for the calibration, to the average dose absorbed by the dosimeter. If not specified particularly, dose values always refer to estimated dose in the dosimeter material in this present work. Dose and dose rate information for this irradiation campaign including irradiation time for each sample is given in Table 2.

Table 2: Summery of the second irradiation campaign aiming to assess different dose effect at constant dose rate.

Sample Name	Dose Rate	Total Dose	Irradiation time
D1 (Dose 1)	2.159 Gy/s	1.30 kGy	10 min

D2 (Dose 2)	2.159 Gy/s	12.91 kGy	99 min 40 sec
D3 (Dose 3)	2.159 Gy/s	77.72 kGy	10 hr
D4 (Dose 4)	2.159 Gy/s	0.47 MGy	60 hr

A picture of all the irradiated sample listed in Table 2 is given in Figure 3. 3. As expected, color of samples changes after irradiation, becoming progressively darker.

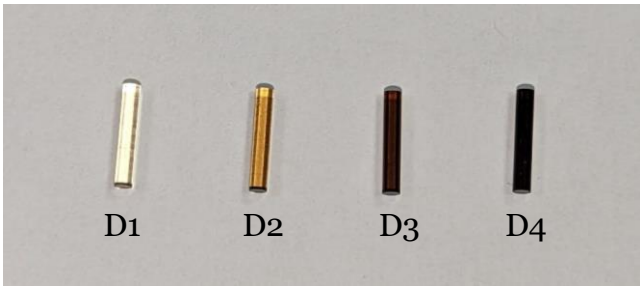

Figure 3. 3 : D1, D2, D3 and D4 samples after irradiation.

3.3.1 Dose effect during irradiation

Spectral RIA as a function of the dose is shown for D1, D2, D3 and D4 samples in Figure 3. 4 (a). This figure shows that the transmission window for 0.47 MGy sample, D4 becomes narrower due to higher attenuation at relatively lower wavelengths, approximately below 650 nm. To better compare RIA increase for the four samples, as an example, RIA kinetics is plotted at 700 nm wavelength as a function of absorbed dose in Figure 3. 4 (b), as at this wavelength provides the RIA data up to 0.47 MGy dose range.

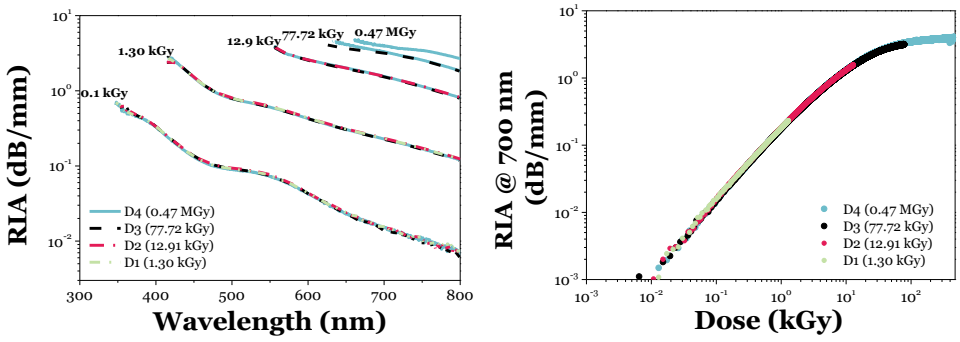

(a) (b)

Figure 3. 4: (a) Spectral RIA at selected doses, (b) RIA as a function of absorbed dose at 700 nm wavelength.

As expected according to the findings of section 3.1.3, increase in RIA with absorbed dose at all wavelengths is also noticeable in Figure 3. 4 (a). It is worthy to note that increase in RIA for all the sample at difference dose levels is consistent, since the four curves clearly overlap. RIA increases at all wavelengths, including the ones in proximity

of the absorption peak around 560 nm, where the metastable defects and conversion of precursors occurs as discussed in section 3.1.1. This consistency confirms the high reproducibility of measurements in the developed set-up at an identical dose rate.

Figure 3. 4 (b) shows an RIA increase which appears as linear up to a few kGy, approximately 5 kGy. However, RIA growth then starts to slow down at higher dose values, and eventually tend to approach a saturation level after reaching 50 kGy. At this dose, probably new point defects are no longer created as the dose is quite high. In this plot, dose values ranging over almost four orders of magnitude are reported, describing a very large range of dose variation and for this reason it is plotted in log-log scale, differently from the other RIA kinetics graphs.

As RIA increases in same manner in all the samples at a particular wavelength, the transmittance evolution with dose correspondingly is expected to be identical for all the sample at any specific wavelength. As an example, transmittance decay at 445 nm is plotted in Figure 3. 5.

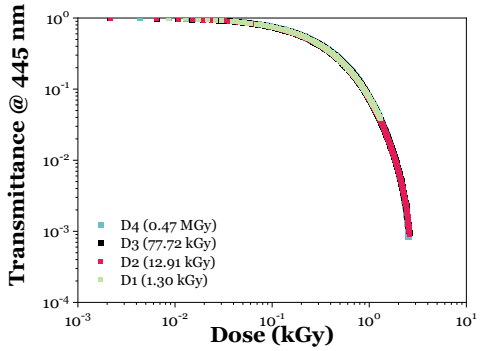

Figure 3. 5: Radiation induced transmittance decay at 445 nm.

Based on Figure 3. 5, the transmitted signal is attenuated to 1% and to 0.1% of its initial value at approximately 2 kGy and 3 kGy of dose in the mentioned irradiation conditions. As transmittance decay a nm at for all the samples is identical as expected, it again confirms the reproducibility of the measurement.

3.3.2 Dose effect after irradiation

In Figure 3. 6, spectral RIA at the end of the irradiation is compared with recovered RIA after 3 hours from the end of the irradiation and the difference between solid lines and dashed lined at each dose level shows the recovery. Comparatively, recovery looks lower at higher doses and in MGy range it looks negligible. The possible reason can that at higher doses metastable defects get enough time to be stabilized during relatively longer irradiation period, required to achieve a higher dose. As a result, the existing defects are only permanent defects.

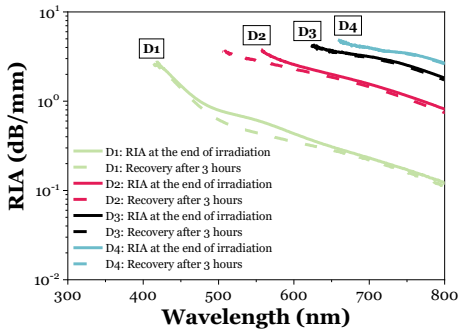

Figure 3. 6: Spectral RIA at highest dose of each sample and their recovery after 3 hours

As shown in Figure 3. 6, highest recovery is observed at wavelengths near 550 nm, while it is comparatively lower below 440 nm and above 700 nm. Aiming to quantify the percentage of recovery, normalized recovery over 9500 second at 445 nm, 560 nm and 700 nm wavelengths are plotted in Figure 3. 7 to cover low to high recovery range.

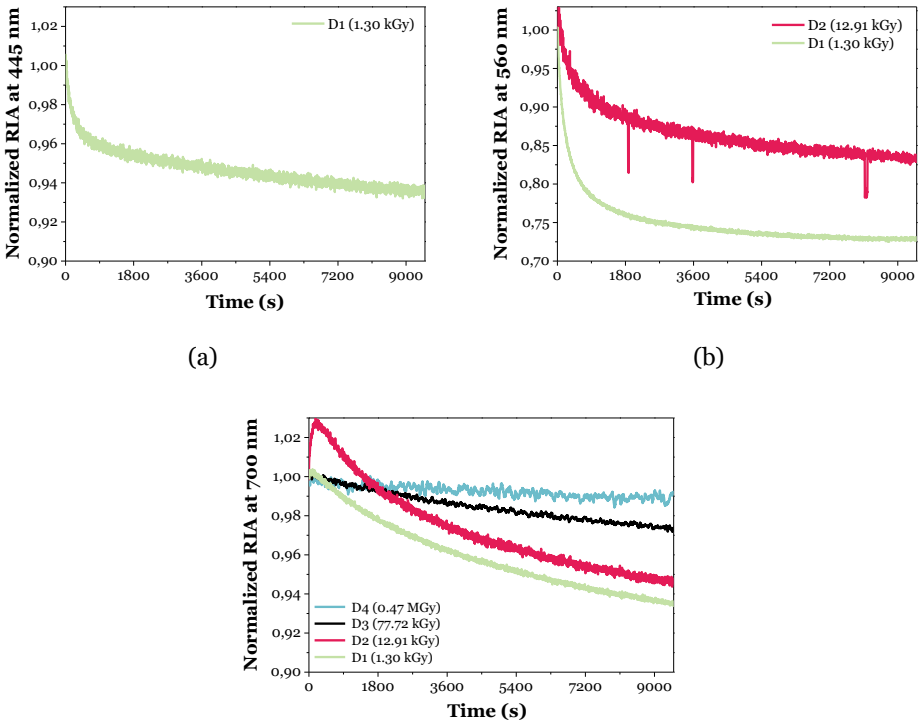

Figure 3. 7: recovery kinetics for 2 hours 30 minutes after irradiation at (a) 445 nm, (b) 560 nm and (c) 700 nm

Figure 3. 7 demonstrates that the higher the dose, the lower the recovery while it is almost negligible at very high doses. For instance, for D4 sample only 1% of recovery is observed at 700 nm wavelength and no recovery is observed at 445 nm and 560 nm. In contrast, higher recovery observed for D1 sample overall varying from 6% to 25% depending on the wavelength within 2 and half hour after irradiation. Moreover, higher

recovery for D1 sample at all the mentioned wavelengths might be also attribute to insufficient time for stabilizing metastable defects during irradiation, corresponding to short exposure. These defects get stabilized after irradiation, leading to a higher recovery in D1 sample.

In Figure 3. 7 (a), 6% recovery is measured at 445 nm at for D1 sample that is irradiated up to 1.3 kGy, corresponding to the mid-dose range, in which dosimetry is assessed based on transmittance. Accordingly, recovery at this wavelength should be accounted for when comparing on-line measurements with passive readout systems.

Although a faster recovery can be observed initially, this process slows down over time. A transient increase in RIA can be observed in Figure 3. 7 (b) and (c), within a few seconds after irradiation is stopped, this phenomenon being particularly noticeable for D2 sample.

3.4 Third irradiation experiment: dose rate dependency

An ideal dosimeter has a response independent on the dose rate. Even though, the lack of data specifically referring to dose rate investigations and the need for further investigation are already been reported in several literatures (in reference [3], [7]), the dose rate dependency of Fd-7 samples, especially in high-dose range has never been thoroughly investigated yet. Possible dose rate dependency must be investigated, as it can lead to errors in dose assessment, in comparison to the reference calibration, that is normally performed in certain dose rate conditions.

In this purpose, four RPL samples were irradiated at four different dose rates to a targeted dose value in high-dose range of 11.34 kGy using MOPERIX facility, varying the dose rate over one order of magnitude between 1.75 Gy/s and 0.175 Gy/s. The irradiation conditions are summarized in Table 3.

Table 3: Summery of irradiation campaign aiming to assess dose rate effect.

Sample Name	Dose Rate	Total Dose	Irradiation time
DR1 (Dose rate 1)	1.75 Gy/s (Highest dose rate)	11.34 kGy	1 hr 48 min
DR2 (Dose rate 2)	0.699 Gy/s (2 times lower than DR1)	11.34 kGy	4 hr 30 min
DR3 (Dose rate 3)	0.35 Gy/s (5 times lower than DR1)	11.34 kGy	9 hr
DR4 (Dose rate 4)	0.175 Gy/s (10 times lower than DR1)	11.34 kGy	18 hr

Picture of all the irradiated sample listed in Table 3 is given in Figure 3. 8. As all the samples were irradiated up to a fixed dose, the color of the samples is identical.

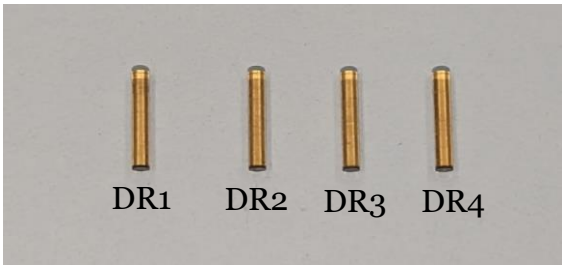

Figure 3. 8 : DR1, DR2, DR3 and DR4 samples after irradiation.

3.4.1 Dose rate effect during irradiation

In Figure 3. 9, spectral RIA at different dose rates (reported in Table 3) at 0.1 kGy, 1 kGy and 11.34 kGy dose levels is plotted.

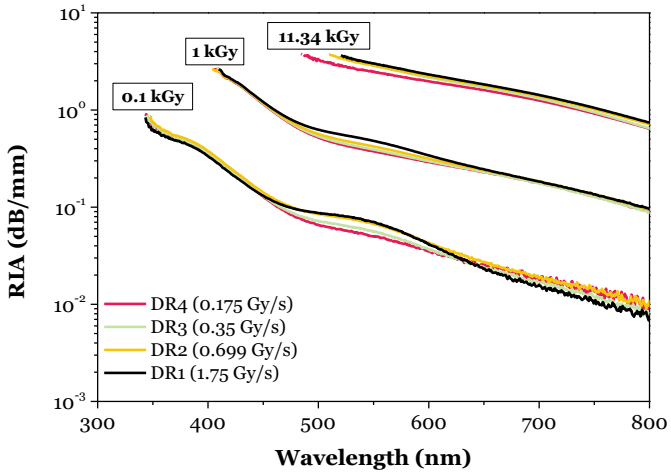

Figure 3. 9: Spectral RIA at different dose rates for the samples listed in Table 3.

Figure 3. 9 shows that the RIA dependence on the dose rate strongly depends on the wavelength. Especially, a significant dose rate effect on RIA is observed between 450 nm-600 nm.

RIA is comparatively higher at higher dose rate for all the observed doses, an exception can be observed at 0.1 kGy above 600 nm. However, dose rate dependency is considerably low around 600 nm - 650 nm and at wavelengths below 450 nm.

Although all samples were irradiated at identical dose, they ended up at different RIA values at the end of irradiation period due to dose rate effect. This phenomenon can be observed more clearly in Figure 3. 12, where the spectral RIA at the end of irradiation for all the samples are plotted in linear scale.

To observe the RIA evolution with absorbed dose for the four investigated dose rates, RIA as a function of dose at 445 nm, 560 nm, 650 nm and 700 nm are plotted in Figure 3. 10.

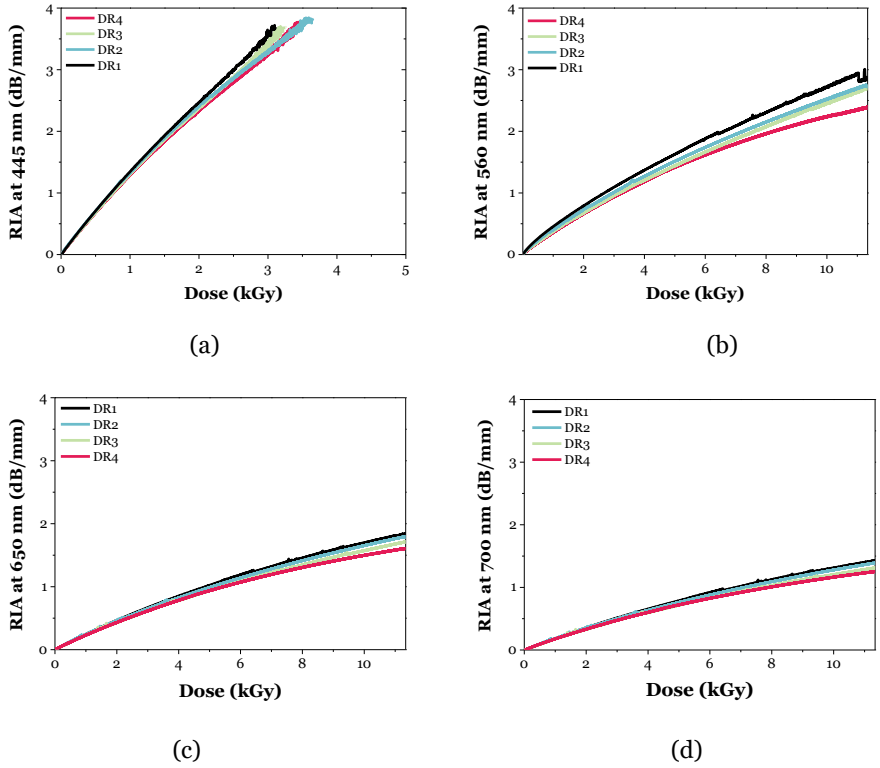

Figure 3. 10: RIA growth as a function of dose at (a) 445 nm, (b) 560 nm, (c) 650 nm and (d) 700 nm for the samples listed in Table 3.

All the plots in Figure 3. 10 can be explained by categorising the dose region into low-mid-high range according to Section 1.2. Among all the plots in Figure 3. 10, the dose rate effect on RIA growth is higher at 560 nm in all the dose ranges, which is quite obvious according to previous discussions. This dependency increases with increase in total dose and the difference in RIA becomes more that 0.5 dB/mm, corresponding to 17% at 11.34 kGy due to variation in dose rate over one order of magnitude.

For other wavelengths, dose rate effect on RIA is negligible at all the selected wavelength, in low-dose range up to 0.3 kGy. The dose rate dependency increases in mid and high dose range in all the wavelength.

In mid-dose range between 0.3 kGy-6kGy, dose rate effect is relatively high for RIA at 445 nm and 700 nm, for example RIA difference is around 11% RIA difference around where at 650 nm this difference is 8%. Moreover, after reaching to 2.5 kGy, RIA value starts to fluctuate and this effect is prominent at lower rate. In high-dose range at 11.34 kGy, RIA difference becomes 13% for both 650 nm and 700 nm. These findings indicates that the dose rate effect on RIA growth is comparatively low between 650 nm -700 nm wavelengths.

According to Figure 3. 9 & Figure 3. 10, higher RIA at high dose rate occurs due to relatively faster dose deposition within a short period creates comparatively higher numbers of stable and metastable point defects, has lesser time to recover those defects during irradiation, leading to a high absorption. This effect makes wavelengths sensitive

to dose rate. Additionally, the dose rate dependency or increase in percentage of RIA difference slows down at high doses, supporting the hypothesis of stabilization in metastable defects or conversion of precursors to other forms with progress of time. This is evident for all wavelengths.

Transmittance decay at 445 nm is plotted in Figure 3. 11 for all four samples listed in Table 3.

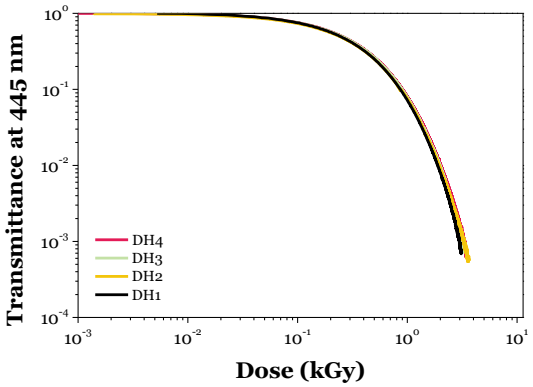

Figure 3. 11: transmittance decay at 445 nm as a function of absorbed dose

Figure 3. *11* confirms the negligible dose rate dependency on radiation matter interaction in FD-7 samples up to 1 kGy at 445 nm during irradiation as transmittance curves for all four samples follows same decay at this wavelength. However, after 1 kGy dose rate starts to affect the transmittance decay at this particular wavelength and the dependency increases with total dose, a supporting agreement can also be observed in Figure 3. 16.

3.4.2 Dose rate effect after irradiation

To observe the effects on after irradiation, RIA at the maximum investigated dose of 11.34 kGy and recovery after 3 hours is plotted in Figure 3. 12 for the four samples, the difference between solid lines and dashed lined at each dose level shows the recovery.

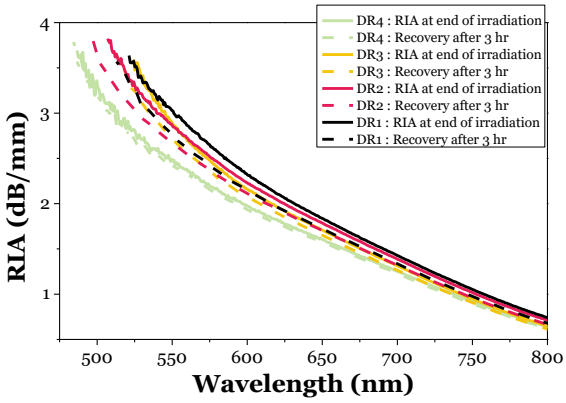

Figure 3. 12: Spectral RIA at highest dose of each sample and their recovery after 3 hours

As expected according to previous findings, Figure 3. 12 also shows a higher recovery within 500 nm- 600 nm wavelengths. Most importantly, D1 sample, irradiated at highest dose rate among the samples compared, has highest recovery at almost every wavelength. Conversely, D4 sample has the lowest recovery, almost negligible. This observation suggests that-

- high dose rate is associated to higher recovery
- as higher dose rate also associated to higher RIA during irradiation, this higher recovery reduces the overall dose rate effect after recovery. Accordingly, the dose rate dependency on passive measurements is correspondingly lower.

Moreover, it confirms the hypothesis relating these phenomena mainly visible at high dose rate, as associated to metastable defect creation and precursor conversion, as discussed in section 3.4.1. Although, samples end up at different RIA levels at the end of irradiation, this RIA difference among the samples reduces after 3 hours of recovery.

In order to quantify the recovery percentage for different dose rate at different wavelength, normalized recovery kinetics over 3 hours after irradiation at 560 nm, 650 nm and 700 nm is presented in Figure 3. 13.

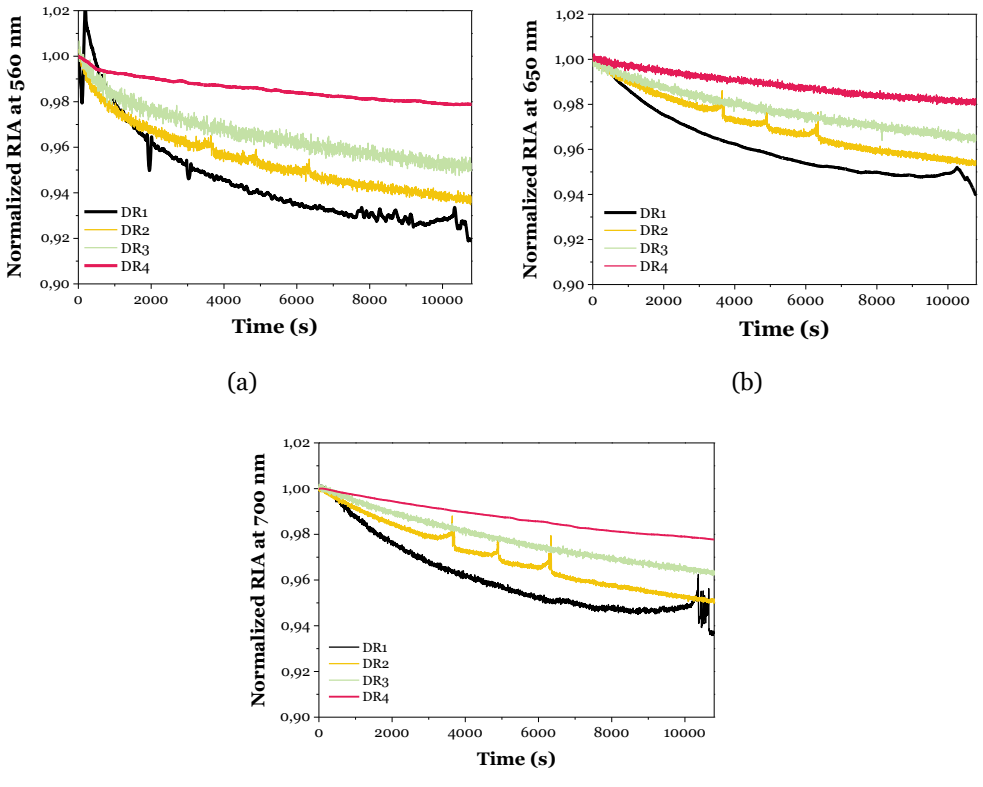

Figure 3. 13: Recovery in each sample at 560 nm, 650 nm and 700 nm within 3 hours of irradiation.

Figure 3. *13* illustrates that DR4 sample has a more gradual recovery, reaching a maximum of 2% within the first 3 hours at all the analysed wavelengths, by contrast, in the observed time scale, recovery varies most for DR1 sample, ranging between 4-8% depending on wavelength. Concerning the recovery kinetics, DR1 recovers faster than other samples. Due to dose rate variation, recovery variation between DR1 and DR4 is recorded 6%, 4% and 3% at 560 nm, 650 nm and 700 nm accordingly after 3 hours the irradiation. Therefore, the following conclusions can be drawn:

- dose rate effect is generally low at 650 nm and 700 nm, or (in between these wavelengths) in comparison to other wavelengths.
- sample irradiated at high dose rate exhibits a faster and relatively higher recovery.

3.5 Post-mortem results

First post-mortem measurement of D2, D3, D4 were performed after 14 days of irradiation while a second post-mortem measurement of D1, D2, D3, D4 was performed after 2 months from the conclusion of the irradiation. Results are shown in Figure 3. *14*. The first post-mortem result post-mortem result for D1 sample is not available due to a technical issue during data acquisition.

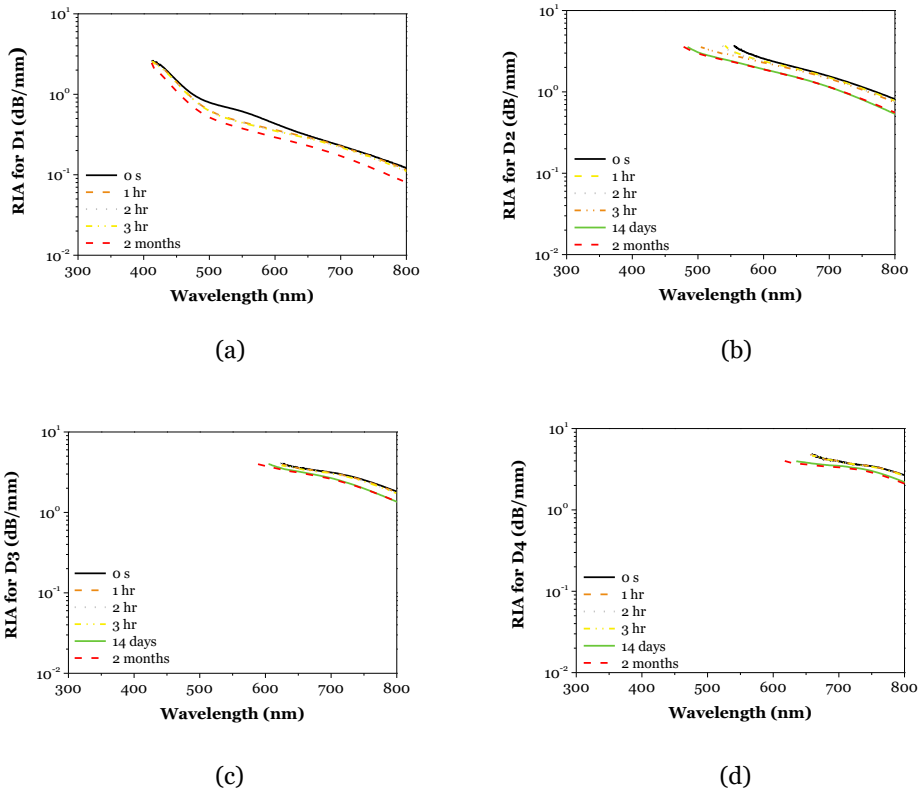

Figure 3. 14: Spectral recovery within 2 months of (a) D1, (b) D2, (c) D3 and (d) D24, measured by performing post-mortem measurement).

Post-mortem measurement of D2, D3 and D4 at 14th day exhibits significant recovery at all wavelengths within the time from irradiation to post mortem measurement before it reaches to a saturation. Furthermore, RIA value after 14 days and 2 months are overlapped completely, indicating that recovery reached its saturation within 14 days, implying that any quantitative measurement (RIA, transmittance etc.) performed at 14th day and after 2 months will provide almost same results. Although the data for D1 is not available, data for other samples suggests that D1 also becomes stabilized by 14 days of post-irradiation.

Further study is required to identify the minimum time for complete recovery and reaching to a saturation, that in the selected irradiation conditions seems shorter than 14 days, and to verify whether the same behaviour is found for DR1 as well, as assumed.

3.6 CERN's Readout

All irradiated dosimeters were sent to CERN for dose readout using the system described in [30], previously calibrated with ^{60}Co source. The so-called actual dose is calculated by multiplying the measured dose rate (using ionising chamber during online measurement at LabHC) with total irradiation time and a factor of 3.7, used for the conversion of the dose in water to the average dose in FD-7. The so-called measured doses, correspond to the outcome of the readout system available at CERN, where the irradiated dosimeters were sent. All these quantities are reported in Table 4 alone with the ratio between the measured and the actual dose.

Table 4: Comparison of actual dose recorded at LabHC and measured dose at CERN.

Sample Name	Dose Rate (Gy/s)	Actual Dose (kGy)	Measured Dose (kGy)	Ratio
D1	2.159	1.30	1.0	0.77
D2	2.159	12.91	12	0.93
D3	2.159	77.72	85.19	1.11
D4	2.159	466	416.9	0.89
DR1	1.75	11.34	10.9	0.96
DR2	0.699	11.34	12.6	1.11
DR3	0.35	11.34	10.7	0.95
DR4	0.175	11.34	11.1	0.98
DR4.1	0.175	1.05	0.94	0.90
DR4.2	0.175	37.8	36.83	0.97

The readout at CERN was performed at distinct intervals after irradiation. Specifically, D1, D2, D3, D4, DR4.2 were read after almost 1 months after irradiation, while DR1, DR2, DR3, DR4, DR4.1 were read within 5-8 days from the conclusion of their irradiation. Relative error on the measured dose correspond to 5% while the one on the actual dose correspond to 30%, mainly depending on the dose homogeneity according to the performed simulations, as described in [30]. For all the samples, a satisfactory agreement between the measured dose and the doses estimated at LabHC is found.

Especially, no particular difference is noticed in dose estimation for samples DR1, DR2, DR3, DR4, confirming negligible dose rate dependency in dose estimation at high-dose range.

In reference to the three different readout areas defined in Section 1.2, all the samples listed in Table 4 absorbed doses belonging to the high-dose range, except for D1 and DR4.1, whose dose lay in the mid-dose range.

In Table 4, the highest deviation in dose estimation correspond to 11% for the samples irradiated at high-dose range. By contrast, a higher deviation of 23% is observed for D1 sample and of 10% for DR4.1 sample. They both belong to the mid-range, but D1 has been read after 1 months from the irradiation conclusion, while DR4.1 after 4-5 days only. In mid-range, dose is assessed using transmittance, so different time intervals between irradiation and readout might affect the dose readout. Recovery phenomena might accordingly affect dose estimation in this rage.

To verify this, percentage of recovery at 445 nm wavelength for D1 sample is quantified from post-mortem measurement after 2 months of irradiation (plotted in Figure 3. 14 (a)). Acquired result is presented in Table *5*. However, the post-mortem measurement for DR4.1 is not available due to technical issues during the experiment.

Table 5: Percentage of RIA recovery for D1 sample over 2 months in comparison to the RIA at the end of the irradiation.

Sample name	Recovery after 1 hr	Recovery after 2 hr	Recovery after 3 hr	Recovery after 2 months
D1	4.49%	5.63%	5.87%	26.29%

Data in Table *5* confirms that 26% RIA recovery is observed in sample D1 after 2 month of recovery time. According to the post-mortem result of D1 sample after 2 months of irradiation, transmittance at 445 nm becomes 0.0965 which corresponds to a dose value of 0.9 kGy instead of 1.3 kGy. based on the data collected during irradiation (online). As the post-mortem measurement is one kind of passive measurement, this analysis confirms that recovery influences passive dosimetry in mid-dose range. This demands a further investigation of dose and dose rate dependency on recovery in this particular dose range.

3.7 Fourth irradiation experiment: Mid-range recovery study

The study presented in Section 3.5 shows the necessity of recovery investigation in mid-range, to a more reliable and more accurate dose estimation. It has already been discussed in Section 3.2 and in Section 3.3 that recovery is time, dose, and dose rate dependent. Even though, recovery becomes time independent after reaching to a saturation value according to post-mortem measurement in Section 3.4, accurate quantification of this phenomenon remains a challenging task, that will be the aim of future studies.

In this experiment, 4 FD-7 samples (M11, M21, M31, M41) were irradiated using IDFix facility at doses ranging from 0.3 kGy to 5.097 kGy to cover the mid-dose range (corresponding to 0.3 kGy -6 kGy) at a constant dose rate of 1.036 Gy/s. The study aims at investigating the different dose effect on transmittance and recovery in this range. Furthermore, 2 more samples (M22 and M32) were irradiated at a constant dose rate of 0.2072 Gy/s (5 times lower than 1.036 Gy/s) to observe the dose rate effect at two targeted doses, corresponding to the ones delivered to samples M21 and M31. All information regarding this irradiation campaign is summarised in Table 6.

Table 6: Summary of mid-dose range investigation.

Sample name	Total Dose (kGy)	Dose rate (Gy/s)	Irradiation time
M11	0.37	1.036	6 min
M21	1.06	1.036	17 min
M22		0.2072	1 hr 25 min
M31	3.11	1.036	50 min
M32		0.2072	4 hr 10 min
M41	5.10	1.036	1 hr 22 min

Dose and dose rate effect on transmittance recovery at 445 nm for all the mentioned samples is summarized in Table *7*.

Table 7: Summarized transmittance result at 445 nm wavelength for all the samples.

Sample name	Transmittance at 445 nm after irradiation			Recovery in transmittance	Actual dose	Dose after recovery	Error
	0 s	3 hours	10 hours				
M11	0.396	0.415	N/A	5%	0.37	0.35	6%
M21	0.089	0.098	N/A	10%	1.06	1.01	5%
M22	0.094	0.104	N/A	10%		1.01	5%
M31	N/A	N/A	0.0016	**Cannot be calculated**	3.11	2.73	13%
M32	N/A	0.001	0.0022			2.77	11%
M41	N/A	N/A	0.0015		5.10	3.32	35%

In Table *7*, recovery of transmittance at 445 is around 5% for M11 sample, corresponds to 6% underestimation of dose after 3 hours of post-irradiation, where for M21 recovery of transmittance is 10% and underestimation of dose is 5%. Moreover, no dose rate effect is observed, as M21 and M22 samples exhibit the same recovery, in percentage, after 3 hours.

It was not possible to assess transmittance recovery at 445 nm for M31, M32 and M41 samples, as the RIA saturates and cannot be measured at the end of the irradiation. To quantify the percentage of recovery in transmittance, transmittance at highest absorbed dose (i.e., corresponding to the end of the irradiation) is considered as refence value. In

the realised experiments, signal at 445 nm get completely absorbed by the sample approximately at 3 kGy. In therefore, for the samples total dose above 3 kGy do not have any refence transmittance at 445 nm, making it impossible to calculate the percentage of recovery or improvement. However, comparing the transmittance after 10 hours of recovery with online measurement data for M31, M32 and M41, error in dose estimation is determined in Table *7* this estimation cannot be possible with offline measurement alone, also a remarkable error can be occurred due to higher fluctuation.

In order to address this limitation, beside transmittance measurement at 445 nm, RIA measurement at higher wavelength, which are less affected by dose and dose rate be considered. In this purpose, recovery of RIA in all the listed samples is studied also at 630 nm, and 700 nm, as examples of possible wavelengths that could provide complementary information to recovery at 445 nm alone, aiming at improving the general understanding of recovery mechanisms and its possible impact on the dose readout in mid-range. The study presented below will help to evaluate the usability of these wavelengths in targeted application.

Recovery in RIA at 445 nm, 650 nm and 700 nm for the samples listed in Table 6 are given in Table 8.

Table 8: Post-irradiation recovery over time at 445 nm, 650 nm, and 700 nm. Percentage values or recovery refer to the values measured after 3 hours.

Sample name	**Recovery at 445 nm**				**Recovery at 650 nm**			**Recovery at 700 nm**		
	0 s	**3 hr**	**10 hr**	**In (%)**	**0 s**	**3 hr**	**In (%)**	**0 s**	**3 hr**	**In (%)**
M11	0.466	0.442	-	5	0.082	0.077	6	0.061	0.060	3
M21	1.211	1.168	-	4	0.222	0.206	8	0.170	0.162	5
M22	1.188	1.140	-	4	0.213	0.189	5	0.164	0.145	12
M31	3.232	2.875	-	12	0.578	0.533	8	0.445	0.409	9
M32	-	3.092	-	5 (at 446 nm)	0.575	0.554	4	0.448	0.429	5
M41	-	-	3.63	**Can not be calcu-lated**	0.914	0.862	6	0.713	0.670	6

In Table 8, recovery at 445 for M32 correspond to 5% based on the immediate next wavelength 446 nm as the reference for that wavelength is available. On the other hand, there was no recover value for sample M41 within first 3 hour. Interestingly, recovery is observed after 10 hours. To visualise the dose effect on recovery in mid-dose range, percentage of recovery at mentioned wavelengths for all the sample irradiated at an identical dose rate of 0.28 Gy/s are plotted in Figure 3. 15.

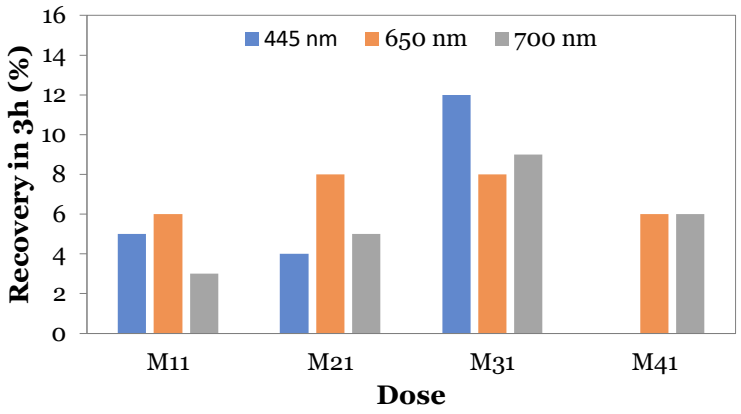

Figure 3. 15: Percentage of recovery as a function of dose within 3h for M11, M21, M31, M41 samples at 445 nm, 650 nm, and 700 nm.

Figure 3. 15 represents that the recovery rate at 445 nm in mid-dose range varies over a wide range between 4% - 12%, for M11, M21 and M31, indicating dose variation between 0.37 kGy and 3.11 kGy. This variation is lower at 700 nm, around 3% - 8% for all the samples, dose varying from 0.37 kGy to 5.10 kGy. On the other hand, signal at 650 nm is the most stable in the investigated range, having variations of approximately 2% only.

Further, recovery for M21, M22 (dose 0.37 kGy) and M31, M32 (dose 3.11 kGy) are plotted in Figure 3. 16 to analyse the dose rate dependency.

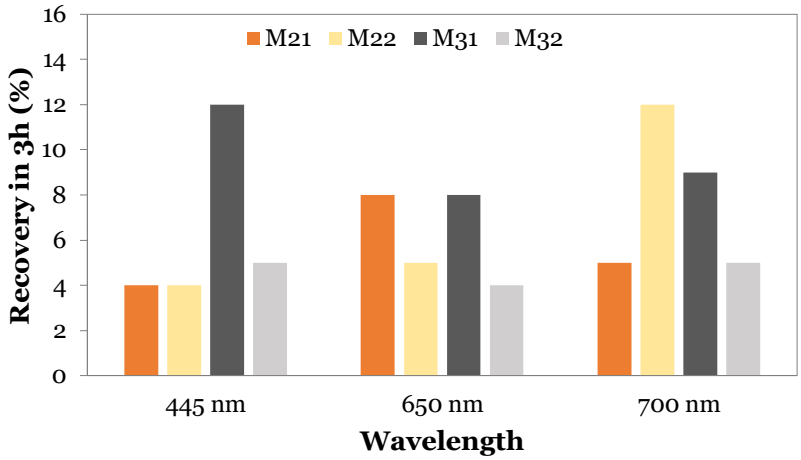

Figure 3. 16: Dose rate dependency: Percentage of recovery as a function of wavelength thin 3h for M21, M22, M31, M32 samples at 445 nm, 650 nm and 700 nm

Although, dose rate dependency at 445 nm is negligible for the samples M21 and M22, irradiated up to 1.06 kGy , it is significantly higher for the samples M31 and M32, irradiated to 3.11 kGy. Contrary, dose rate dependency at 700 nm is higher for M21 and M22 samples where it is relatively lower for samples M31 and M32. However, dose rate dependency at 650 nm seems to have the same behaviour at both dose level: recovery is higher at lower dose rate.

This evidence confirm that recovery has a complex dependence on dose, dose rate and wavelength dependent in mid-range. In this complicated scenario, the analysis of a single wavelength to determine transmittance, which is indeed used to determine the dose, might lead to dose underestimations or overestimations, depending on the actual recovery at the time of the measurement. It is particularly interesting to note that there is almost no dose rate effect for the recovery at 445 nm wavelength at 0.37 kGy, making it ideal for dose assessment in this dose range. By contrast, at the same wavelength, a relevant dose rate effect is reported at 3.11 kGy, possibly leading to errors in dose estimations.

To improve the reliability of mid-dose measurement, complementary information on wavelengths other than 445 nm alone could be helpful. In particular, the following is proposed:

- Multi-wavelength transmittance analysis should be performed;
- Further dose rate studies should be performed to assess the recovery dependence on the dose rate for various selected wavelengths in mid-dose range;
- Dose ranges in which, at a certain wavelength, recovery has a low dose rate dependence should be identified. For instance, depending on the findings in Section 3.4 and 3.7, dose rate dependency is relatively low between 650 nm-700 nm;
- The mid-range could be further divided in sub-regions in which combined different information, such as combination of transmittance with RIA at different wavelengths is used to assess the dose.

Depending on the findings in Section 3.4 and 3.7, considering RIA at a wavelength between 650 nm-700 nm for dose estimation in mid-dose range might be a good option due to relatively low dose rate dependency and less fluctuations in this specific range. However, more comprehensive studies are needed to determine calibrated curves by measuring the RIA offline, after it reaches to the saturation, as it is most important to ensure the stability and repeatability in measurement. To calculate the dose, percentage of recovery at different dose level needs to be compensated to improve accuracy.

Additionally, it is also important to preserve the samples in a temperature-controlled environment to avoid undesirable recovery due to temperature variation. It may also possible that after preserving the samples in a temperature-controlled environment, recovery of irradiated sample will be reduced compared to the result presented in this manuscript as samples reported here as the irradiated samples were not kept in controlled temperature and atmosphere conditions.

3.8 Fifth irradiation experiment: online RPL measurement

Aiming to observe the real-time RPL behaviour during irradiation and after irradiation, two FD-7 samples, namely R1 and R2 were irradiated to 1.06 kGy and 5.28 kGy at IDFix facility. Irradiation conditions are summarized below in Table 9.

Table 9: Summery of irradiation conditions aiming to ossssbserve RPL signal online

Sample Name	Dose Rate	Total Dose	Irradiation time
R1	1.036 Gy/s	1.06 kGy	17 min
R2	1.036 Gy/s	5.28 kGy	1 hr 25 min

The online RPL measurements were performed according to the process described in section 2.6. However, the laser-matter interaction in FD-7 sample was tested offline before performing the online measurement. As the RPL intensity depends on the injected power, at first the RPL signal of a previously irradiated sample was measured at different injected laser power from 1 mW to 9 mW by increasing current from 25 mA to 51 mA. Figure 3. 17 demonstrates that the intensity of RPL signal progressively increases with increase in injected laser power. However, the possibility of photobleaching limits the injection of high power in irradiated samples.

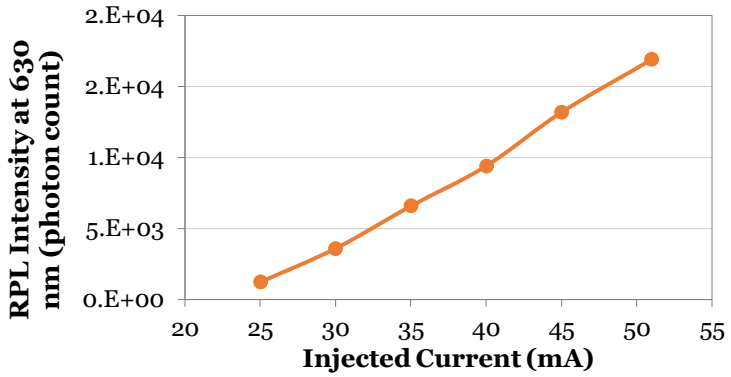

Figure 3. 17: RPL signal at different injected laser power as a function of current

As photobleaching is expected to be depended on the power of injected light and duration of illumination, the bleaching effect was previously tested on another available irradiated sample to identify a reasonable power and time threshold to operate the laser avoiding any significant alteration of the RPL signal due to photobleaching.

To observe the bleaching effect, an irradiated sample was illuminated for 1 hours in offline at 51 mA laser operating current. The acquired result is plotted in Figure 3. 18.

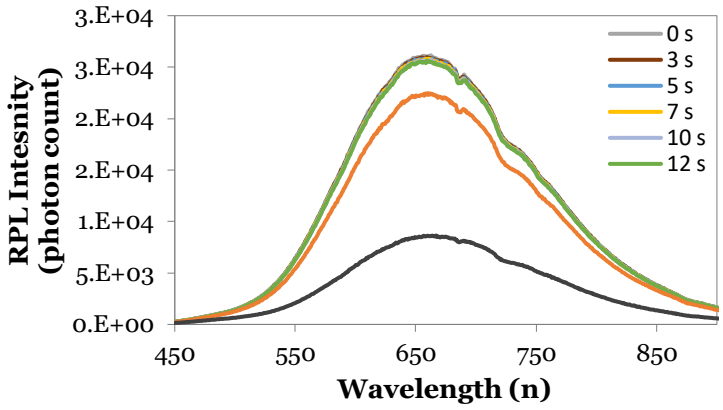

Figure 3. 18: RPL signal evolution with time at injected laser current of 51 mA

Figure 3. 18 shows that the RPL signal decays significantly over time at an injected current of 51 mA, corresponding to 9 mW power. However, the signal exhibits satisfying stability with a deviation less than 1.5%, for the first few seconds of irradiation (around 10 s). This suggests that instead of operating in continuous wave (CW), injecting laser pulses of 10 seconds at 51 mA operating current allows to achieve high RPL signal limiting the bleaching effect.

For RPL signal acquisition online, R1 sample was irradiated up to 1.06 kGy total dose, placing the RPL on the dedicated set-up as described in Section 2.6. During irradiation, RPL centres were excited with a pulse of 10 s duration, operating at 51 mA current. The interval between two following pulses is not constant, as the laser was operated manually. After finishing irradiation, the RPL signal was collected for another 20 minutes.

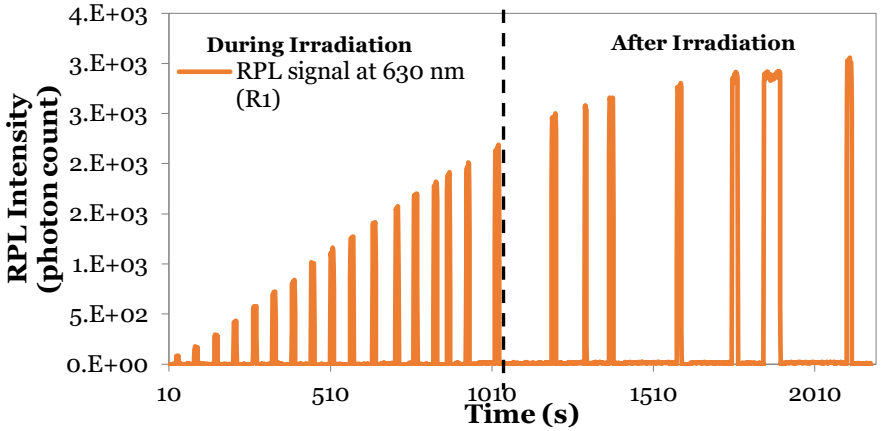

Figure 3. 19: RPL signal of R1 sample at 630 nm evolution with time during and after irradiation

In Figure 3. 19, RPL signal intensity increases with absorbed dose, this corresponds to the proportional formation of RPL centres. As expected according to literature [7], this process continues even after the irradiation stops. Even though, the increase in intensity gradually slows down but it does not reach to any constant value within 20 minutes. Offline RPL signal readout was performed after 14 hours of the irradiation as well. The measured RPL signal intensity was stabilized to value which 13% higher than the intensity obtained at the end of irradiation.

R2 sample was irradiated in same conditions up to 5.28 kGy, intending to cover the mid-dose. Evolution of RPL signal over time at 630 nm presented in Figure 3. 20. However, the sample and integration time of data acquisition was not identical for R1 and R2, direct comparison of the photon count between these two curves is not possible.

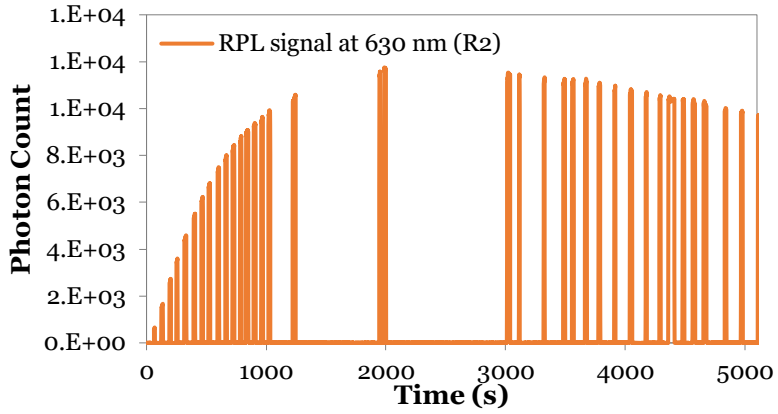

Figure 3. 20: RPL signal for R2 sample evolution with time at 450 nm and 630 nm during and after irradiation

Figure 3. 20 illustrates that RPL intensity at 630 nm increases with absorbed dose up to 2 kGy during irradiation. However, the signal starts to decay after 2000 seconds 2 kGy. As it is observed in the previous study that the RPL signal increases even after the irradiation session ends and end up to a higher intensity, the RPL signal the RPL_5k irradiated sample was measured after 12 hours of post-irradiation to observe the behaviour. Interestingly, this measurement shows that RPL signal was settled to a constant value around 9% lower than the intensity recorded at highest dose during irradiation. This phenomenon is observed for the first time as online measurement of RPL signal at this comparatively higher dose is performed for the first time.

Despite the different irradiation conditions, an attempt is made to compare the results here collected with the ones collected by CERN and available in [3] to achieve better insights of difference between RPL online and offline measurement.

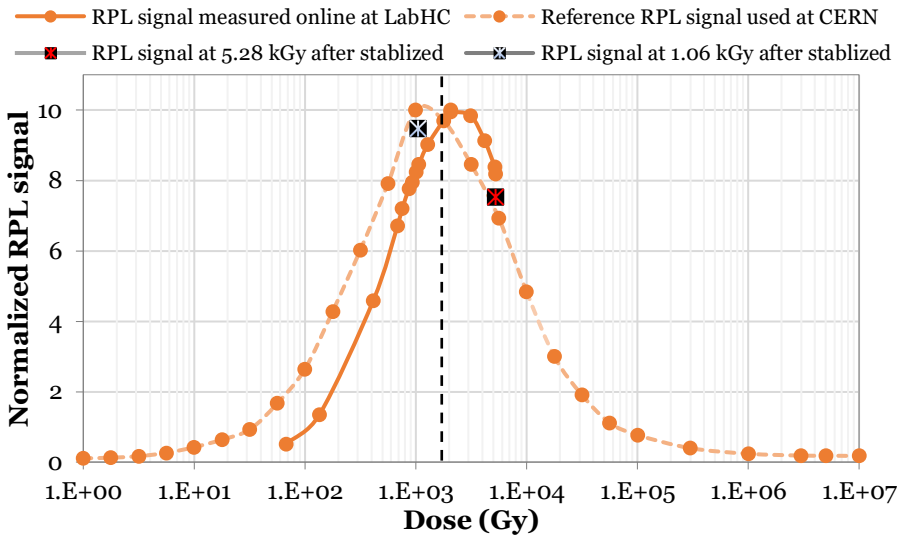

Figure 3. 21: Comparing RPL signal of R2 sample from online measurement at LabHC with the reference RPL signal from passive measurement, use at CERN

In Figure 3. 21,the result obtained for RPL measurement shows qualitatively same behaviour to the reference curve is used at CERN with a shift in the peak position. However, this is agreeable, as the RPL signal stabilizes to a new value 12 hours after irradiation. It is noteworthy that RPL signal at 1.06 kGy, before 1.8 kGy settles to a higher value after 12 hours from irradiation conclusion whereas RPL signal at 5.28 kGy, after 1.8 kGy settles to a lower intensity; eventually getting closer to the reference value use at CERN. This considered, the replication of the phenomena previously observed can be considered as very encouraging and satisfactory, especially considering that RPL measurements were performed online in a totally different environment with a different set-up following different method in the frame of the present work.

A combined curve of the online measurements including the reference data used at CERN is plotted in Figure 3. 22, similar as the Figure 1. 5 (a). In the following plot, RIA at 650 nm is also included as a better result was obtained at this wavelength in previous sections.

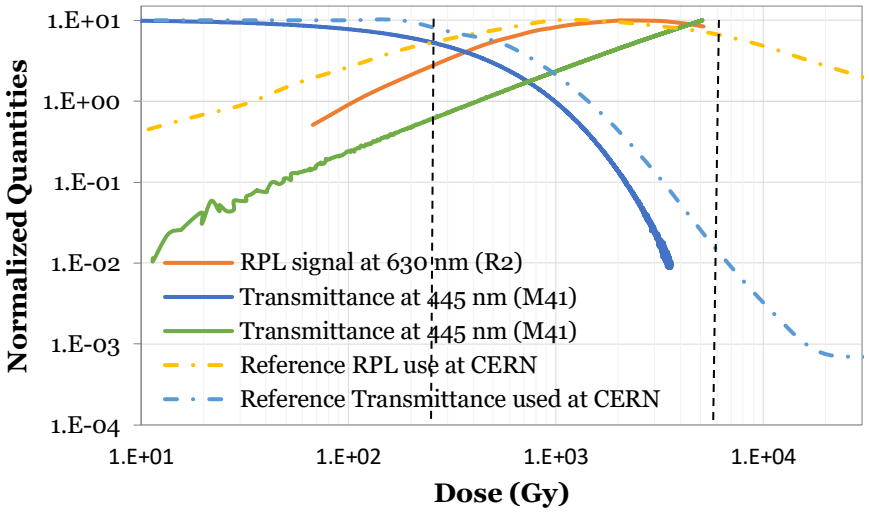

Figure 3. 22: Calibrated curve for mid-dose range measurement, generated using data produced during irradiation of RPL_5k and M41 samples.

In Figure 3. 22, low-dose range and mid-dose range are separated with dashed line according to the ranges mentioned in Section 1.2.

In this plot, transmittance curve of 445 nm wavelength used at CERN exhibit higher values at specific a dose than the transmittance obtained during online measurement. This a validation of the hypothesis that transmittance at 445 nm will be stabilized to a higher value after reaching to the saturation of recovery. The RPL signal will also shift near the peak of the reference after settling.

This suggests that calibration for passive measurement (when the RPL signal is settled, and transmittance is recovered completely) ensures the stability in measurement. However, it might cause error in dose estimation as the post- irradiation effects are not taken in account properly, especially in dose measurement in mid-dose range alone with

transmittance at 445 nm, as inaccuracies may occur in percentage of recovery calculation due to unstable refence value after 2kGy.

Furthermore, based on the results collected in this work, RIA at 650 nm seems to exhibit better linearity and stability in mid dose range compared to transmittance at 445 nm. This encourages to consider the proposal of using RIA at a wavelength between 650 nm – 700 nm for mid rage dose estimation, as described in Section 3.8.

3.9 Offline RPL readout with confocal microscope: effect of Al filter

In the present work, two FD-7 samples were irradiated, one without any filter and another with 1.5 mm Al filter configurations in order to observe the effect of 1.5 mm Al filter on RPL centre creation within both the samples in microscopic scale using LabRAM ARAMIS confocal microscope. RPL signal and color map obtained from confocal microscopy for without filter and with Al filter configurations is given in figure 3.4 and in Figure 3. 23 respectively.

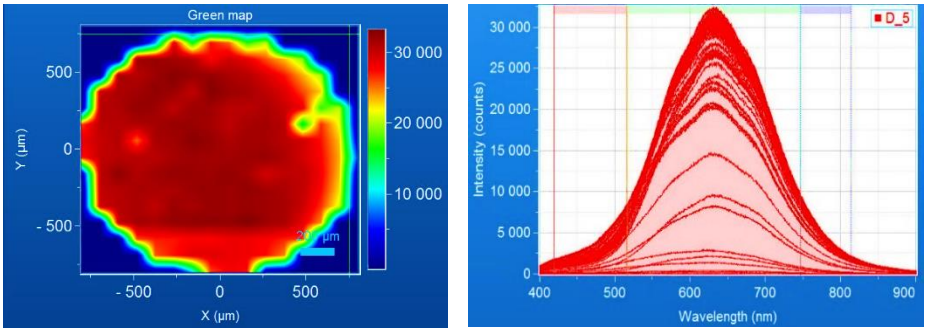

(a) (b)

Figure 3. 23: (a) Color map of dose distribution in FD-7 sample irradiated in without any filter configuration and (b) RPL signal collected by confocal microscope

Figure 3. 23 (a) represents dose distribution throughout the sample using color map. In the plot, the upper left corner of the sample exhibits darker shade of red color, indicating the presence of higher number of RPL centre in this region. Other sides having lighter shade is the evidence of comparatively a smaller number of RPL centres. Random imperfections that emerged during manufacturing, are also noticeable across the sample.

Based on the information provided by the color bar and Figure 3. 23 (b), photon counts below 10000 indicates region outside the sample area. Conversely, photon count from 10000 to around 25000 corresponds to the sample edges and local imperfections. Therefore, photon count up to 25000 are disregarded while investigating uniformity. Overall, the photon count varies from 25000 to almost 35000 over the sample.

However, Figure 3. 24 (a) exhibits significant regularity in color shades throughout the sample. Furthermore, the color bar and Figure 3. 24 (b) suggests that photon count up to 22500 corresponds to imperfections, surface region and the area outside the sample.

Hence, the photon count across the sample area varies from 22500 to approximately 26000.

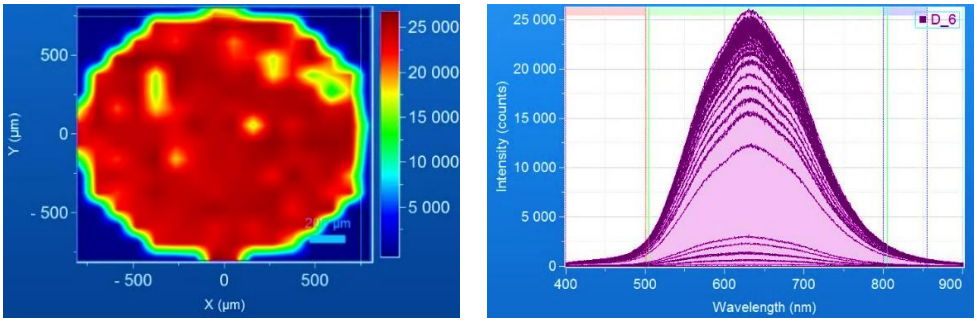

(a) (b)

Figure 3. 24: (a) Color map of dose distribution in FD-7 sample irradiated in with Al filter configuration and (b) RPL signal collected by exciting RPL centres at different points in the sample

In conclusion, introducing a 1.5 mm Al filter in between source and sample has reduced the deviation in photon counts from 10000 to 3500.

However, exact density of RPL centres at a specific position cannot be observed in this process, accordingly inhomogeneity in dose distribution throughout the sample can also not be quantified. The result can be improved by reducing the confocal hole of injected laser light.

Chapter 4. Conclusions and Future Work

4.1 Summary and Conclusions

This study focuses on the characterisation of RPL dosimeters during and after X-ray irradiation, aiming at further understanding their response and its dependence on several parameters.

Customized set-ups were designed, adapted and developed for passive measurement as well as real-time investigation of different radiation-induced quantities. Five different experimental irradiation campaign were successfully realized, targeting the measurement of RIA, transmittance, recovery, post-mortem response and RPL signal. While RPL signal alone is generally used for dose determination in low dose ranges, a combined analysis of these quantities is necessary for a correct dose estimation in mid dose range (approximately between 0.3 kGy and 6 kGy) to high dose range (approximately above 6 kGy). The mentioned quantities have been characterized as a function of the dose and of the dose rate over a wide range of explored values, in the radiation fields produced by a commercial X-ray tube.

The first new set-up successfully established for both offline and real-time RIA measurement allows reliable measurement to be performed with satisfactory repeatability. The second set-up developed for RPL measurement, although operational and already used to measure the first samples, is still under development and has margins of improvement.

Specific irradiations were realized, especially targeting mid and high dose ranges, so far lacking a systematic and complete investigation using X-rays. In the study, FD-7 samples have been irradiated up to a maximum dose of 0.5 MGy, a dose level rarely investigated before and generally speaking not easy to be reached with X-ray radiation, requiring relatively long exposure times and facility time allocation. The sample behaviour has been observed online during irradiation and it was followed up after irradiation, recovery and post-mortem measurements being performed over a period of time up to 2 months after irradiation.

All the collected results present a coherent scenario, in satisfactory agreement with the expectations and with the existing literature. Summary of all investigation shows that, as expected, RIA generally increases with total absorbed dose at all wavelengths, the increase rate depending on total dose, dose rate and wavelength. It is observed that RIA is generally higher at higher dose rates. Correspondingly, transmittance generally decreases as a function of the total absorbed dose, showing a dependency on dose rate and wavelength as well. One of the most crucial parameters to be observed is recovery, whose correct estimation is crucial for the dose assessment in mid-dose range. Recovery is found to be strongly dependent on dose, dose rate, wavelength, and time. If not properly accounted for, it could lead to errors in the dose determination during the passive readout.

Usually, both RIA growth and recovery have higher variation in correspondence of certain wavelengths. Even though the quantities measured in this work do not allow the direct identification of defects, an interpretation based on the evolution of RIA and recovery has been attempted. The wavelengths corresponding to the higher variations can in fact be associated to the presence of optical absorption bands of specific metastable defect. The metastable defect formation and possible recovery after irradiation is affected by dose rate, high dose rates creating more defects within a shorter period time in comparison to low dose rates. In shorter irradiation times, defects might not have time enough to stabilize. Consequently, the response at some wavelengths turns out to be strongly dose rate dependent, especially in the range between 500 nm and 600 nm. Additionally, dose rate has significant impact on recovery at almost every wavelength.

In most of the literature it is claimed that RPL dosimetry is dose rate independent. The experiments realized in this work, especially the ones targeting the mid-range, evidence of possible dose rate effects on RIA, recovery and transmittance at certain doses and for certain wavelengths. For example, transmittance decay at 445 nm during irradiation has negligible dose rate dependency as well, but recovery shows a dose rate dependency, this possibly influencing the dose readout.

The collected results highlight possible differences in dose estimation in mid-dose range when online and passive systems are compared, depending on the time interval between irradiation and readout. Accordingly, and to account for these possible differences. To address these problems, a new approach has been proposed, consisting in the integration of the information on transmittance at 445 nm with the use of other complementary quantities, such as RIA values different wavelengths. For example, 650 nm has been identified as a promising, as at this wavelength the dose rate has relatively low impact on the RIA and on the recovery at certain dose values in the mid-dose range. the proposed method, to be further developed in future studies, might enhance the dosimetry accuracy in this specific range.

Preliminary investigations on the distribution of the RPL centres via confocal microscopy, suggest the possibility of exploring possible inhomogeneities in the distribution of RPL centres within the sample volume. To improve homogeneity, a 1.5 mm thick Al filter to shield the X-ray spectrum was used in most of the performed irradiations.

In addition to the specific considerations on the radiation response of RPL dosimeters, the study clearly proves that commercial X-ray sources can be effectively used for the irradiation of RPL dosimeters and potentially of any other material or component having a thickness at least in the millimetre range, with satisfactory homogeneity. This suggest that X-ray facilities can be considered as possible alternatives to gamma sources and other irradiation facilities concerning the irradiation of various samples and systems up to high doses, in the MGy dose range, and relatively high dose rates in the kGy/h range.

In conclusion, all the objective of this study has been carried out successfully. The reported findings provide valuable information for improving the accuracy of dose estimation, indicating the possibility of systematically extending the application of RPL dosimeters in mid-high dose range for a variety of possible new radiation applications.

4.2 Future work

Although, RPL dosimetry is well established for low dose applications, it is still in its premature stage of research for mid to high dose measurement. In future, more comprehensive studies are highly recommended to broaden the understanding and improve the accuracy of RPL dosimetry in the mentioned dose regions.

Despite the satisfactory results collected and presented in the present work, the set-up realized for RPL measurement still is in preliminary stage. Several improvements are required, such as using a self-operating UV laser instead of the near-UV laser, the combined use of a photo-multiplier with a filter to suppress the laser signal, the illumination of the whole sample volume to collect the maximum RPL signal. For RPL experiment, use of a dedicated sample holder may significantly improve the repeatability and reliability of the measurement. Further improvise can be made by introducing a new set-up for parallel investigation of RIA and RPL measurements via the possible realization of a single, compact and stable integrated set-up, in order to save time and improve repeatability and reproducibility of the measurements.

In future, RIA and recovery evolution at 650 nm and other wavelengths need to be investigated as a function of the dose, of the dose rate and of other irradiation parameters for testing and validation of the proposed method. Furthermore, a calibrated reference curve can be produced by using passive measurement data of RPL signal, transmittance and RIA as a function of dose at various wavelengths. Further experiments and considerations on recovery will allow improvements, especially targeting mid-range dosimetry.

The performed RIA measurements provide a general information on the different existing absorption bands. However, the specific origin leading to these absorptions are not identified yet. Future research can be carried out to identify the specific color centres responsible for the observed absorption bands.

Beside ^{60}Co and X-ray sources, characterisation of these dos78imeters response using other types of irradiation sources can improve the understanding of RPL dosimetry for a variety of applications, including mixed radiation field environments.

Stability of RPL signal after irradiation and fading effect at different dose level requires further studies as well.

Other future work can target the thermal and photo-bleaching effect on irradiated sample, investigating different annealing process and temperature dependency.

References

[1] F. H. Attix, *Introduction to Radiological Physics and Radiation Dosimetry*, 1st ed. Wiley, 1986. doi: 10.1002/9783527617135.

[2] D. Di Francesca *et al.*, "Distributed Optical Fiber Radiation Sensing in the Proton Synchrotron Booster at CERN," *IEEE Trans. Nucl. Sci.*, vol. 65, no. 8, pp. 1639–1644, Aug. 2018, doi: 10.1109/TNS.2018.2818760.

[3] D. Pramberger, Y. Q. Aguiar, J. Trummer, and H. Vincke, "Characterization of Radio-Photo-Luminescence (RPL) Dosimeters as Radiation Monitors in the CERN Accelerator Complex," *IEEE Trans. Nucl. Sci.*, vol. 69, no. 7, pp. 1618–1624, Jul. 2022, doi: 10.1109/TNS.2022.3174784.

[4] H. Schonbacher, M. Furstner, and H. Vincke, "High-level dosimetric methods," *Radiat. Prot. Dosimetry*, vol. 137, no. 1–2, pp. 83–93, Nov. 2009, doi: 10.1093/rpd/ncp195.

[5] H. Vincke *et al.*, "Response of alanine and radio-photo-luminescence dosemeters to mixed high-energy radiation fields," *Radiat. Prot. Dosimetry*, vol. 125, no. 1–4, pp. 340–344, Dec. 2006, doi: 10.1093/rpd/ncm157.

[6] H. Vinke and J. Trummer, "Apparatus and method for determining a dose of ionizing radiation." WO Patent 2 014 161 732, Sep. 10, 2014.

[7] T. Yamamoto, A. Rosenfeld, T. Kron, F. d'Errico, and M. Moscovitch, "RPL Dosimetry: Principles and Applications," presented at the CONCEPTS AND TRENDS IN MEDICAL RADIATION DOSIMETRY: Proceedings of SSD Summer School, Wollongong, Australia, 2011, pp. 217–230. doi: 10.1063/1.3576169.

[8] D. Y.C. and S.-M. Hsu, "Radio-Photoluminescence Glass Dosimeter (RPLGD)," in *Advances in Cancer Therapy*, H. Gali-Muhtasib, Ed., InTech, 2011. doi: 10.5772/23710.

[9] J. Harb *et al.*, "Femtosecond Direct Laser Writing of Silver Clusters in Phosphate Glasses for X-ray Spatially-Resolved Dosimetry," *Chemosensors*, vol. 10, no. 3, p. 110, Mar. 2022, doi: 10.3390/chemosensors10030110.

[10] M. Ferrari *et al.*, "'Radiation to Materials' at CERN," *IEEE Trans. Nucl. Sci.*, vol. 70, no. 8, pp. 1580–1586, Aug. 2023, doi: 10.1109/TNS.2023.3241785.

[11] K. Hiramatsu, S. Yoshihashi, S. Kusaka, F. Sato, E. Hoashi, and I. Murata, "Gamma-Ray Dose Measurement with Radio-Photoluminescence Glass Dosimeter in Mixed Radiation Field for BNCT," *EPJ Web Conf.*, vol. 153, p. 04009, 2017, doi: 10.1051/epjconf/201715304009.

[12] J. Trummer, "Characterisation of CERN's High Level Dosimetry Radio-Photo-Luminescence readout system." technical note provided by CERN.

[13] T. Yamamoto, Y. Yanagida-Miyamoto, T. Iida, and H. Nanto, "Current status and future prospect of RPL glass dosimeter," *Radiat. Meas.*, vol. 136, p. 106363, Aug. 2020, doi: 10.1016/j.radmeas.2020.106363.

[14] T. Kurobori, “Performance characterisation of a real-time fiber dosimetry system using radiophotoluminescent glasses,” *Jpn. J. Appl. Phys.*, vol. 57, no. 10, p. 106402, Oct. 2018, doi: 10.7567/JJAP.57.106402.

[15] D. Pramberger and Y. Q. Aguiar, “Analysis of the High-Temperature Annealing Regeneration Process of the FD7 RPL glass dosimeters.”

[16] “Dose-Ace data sheet 5th edition.” [Online]. Available: https://www.c-technol.co.jp/en/pdf/Dose-Ace_5th_Edition.pdf

[17] M. Fuerstner, D. Forkel-Wirth, H. Vincke, S. Mayer, I. Brunner, and I. Floret, “High-Level Dosimetry systems used at CERN.”

[18] Y. Q. Aguiar, “User Guideline for High-Level Dosimetry (RPL and PAD).” user guide provided by CERN.

[19] G. Okada, Y. Koguchi, T. Yanagida, S. Kasap, and H. Nanto, “Recent advances in radiophotoluminescence materials for luminescence dosimetry,” *Jpn. J. Appl. Phys.*, vol. 62, no. 1, p. 010609, Jan. 2023, doi: 10.35848/1347-4065/ac9023.

[20] Y. Ihara *et al.*, “A compact system for measurement of radiophotoluminescence of phosphate glass dosimeter,” *Radiat. Meas.*, vol. 43, no. 2–6, pp. 542–545, Feb. 2008, doi: 10.1016/j.radmeas.2007.11.045.

[21] S. Girard *et al.*, “Radiation Effects on Silica-Based Optical Fibers: Recent Advances and Future Challenges,” *IEEE Trans. Nucl. Sci.*, vol. 60, no. 3, pp. 2015–2036, Jun. 2013, doi: 10.1109/TNS.2012.2235464.

[22] S. Girard *et al.*, “Recent advances in radiation-hardened fiber-based technologies for space applications,” *J. Opt.*, vol. 20, no. 9, p. 093001, Sep. 2018, doi: 10.1088/2040-8986/aad271.

[23] T. Allanche, “Effect of high radiation doses (MGy) on light Emitting Diodes and optical glasses.” HAL open access archive, Mar. 03, 2021. [Online]. Available: https://www.researchgate.net/publication/351341499

[24] L. Weninger *et al.*, “Calibration in the Visible and Infrared Domains of Multimode Phosphosilicate Optical Fibers for Dosimetry Applications,” *IEEE Trans. Nucl. Sci.*, pp. 1–1, 2023, doi: 10.1109/TNS.2023.3252941.

[25] F. Berghmans, B. Brichard, A. F. Fernandez, A. Gusarov, M. V. Uffelen, and S. Girard, “An Introduction to Radiation Effects on Optical Components and Fiber Optic Sensors,” in *Optical Waveguide Sensing and Imaging*, W. J. Bock, I. Gannot, and S. Tanev, Eds., in NATO Science for Peace and Security Series. Dordrecht: Springer Netherlands, 2008, pp. 127–165. doi: 10.1007/978-1-4020-6952-9_6.

[26] S. Girard *et al.*, “Overview of radiation induced point defects in silica-based optical fibers,” *Rev. Phys.*, vol. 4, p. 100032, Nov. 2019, doi: 10.1016/j.revip.2019.100032.

[27] D. Harvey, *Instrumental Analysis (LibreTexts)*. Chemistry LibreTexts, 2021. [Online]. Available: https://chem.libretexts.org/Bookshelves/Analytical_Chemistry/Instrumental_Analysis_(LibreTexts)

[28] S. Girard *et al.*, "Growth and Decay Kinetics of Radiation-Induced Attenuation in Bulk Optical Materials," *IEEE Trans. Nucl. Sci.*, vol. 65, no. 8, pp. 1612–1618, Aug. 2018, doi: 10.1109/TNS.2017.2778318.

[29] A. Meyer, D. Lambert, A. Morana, P. Paillet, A. Boukenter, and S. Girard, "Simulation and Optimization of Optical Fiber Irradiation with X-rays at Different Energies," *Radiation*, vol. 3, no. 1, pp. 58–74, Mar. 2023, doi: 10.3390/radiation3010006.

[30] M. Ferrari *et al.*, "Characterization of Radio-Photo-Luminescence dosimeters under X-ray irradiation, accepted to RADECS 2023 Conference on Radiation and its effects on Components and Systems, in preparation for submission to IEEE TNS."

[31] "PTW-23344 0.23 cm3 Soft X-ray Chamber Datasheet." [Online]. Available: https://www.emf-japan.com/ptw/img/PDF/PTW23344.pdf

[32] A. Morana *et al.*, "Extreme Radiation Sensitivity of Ultra-Low Loss Pure-Silica-Core Optical Fibers at Low Dose Levels and Infrared Wavelengths," *Sensors*, vol. 20, no. 24, p. 7254, Dec. 2020, doi: 10.3390/s20247254.